Design, Synthesis and Biological Evaluation of Novel 2-((2-(4-(Substituted)phenylpiperazin-1-yl)ethyl)amino)-5′-*N*-ethylcarboxamidoadenosines as Potent and Selective Agonists of the A_{2A} Adenosine Receptor

Delia Preti,[§] Pier Giovanni Baraldi,*[§] Giulia Saponaro,[§] Romeo Romagnoli,[§] Mojgan Aghazadeh Tabrizi,[§] Stefania Baraldi,[§] Sandro Cosconati,*[¶] Agostino Bruno,[‡] Ettore Novellino,[‡] Fabrizio Vincenzi,[#] Annalisa Ravani,[#] Pier Andrea Borea[#] and Katia Varani.[#]

[§]*Dipartimento di Scienze Chimiche e Farmaceutiche, Università degli Studi di Ferrara, Via Fossato di Mortara 17, 44121, Italy*

[#]*Dipartimento di Scienze Mediche, Sezione di Farmacologia, Università degli Studi di Ferrara, Via Fossato di Mortara 17, 44121, Italy*

[¶] *DiSTABiF, Seconda Università di Napoli, Via Vivaldi 43, 81100 Caserta, Italy*

[‡]*Dipartimento di Farmacia, Università di Napoli "Federico II", Via D. Montesano 49, 80131 Napoli, Italy*

Abstract

Stimulation of A_{2A} adenosine receptors (AR) promotes anti-inflammatory responses in animal models of allergic rhinitis, asthma, chronic obstructive pulmonary disease and rheumatic diseases. Herein we describe the results of a research program aimed at identifying potent and selective agonists of the A_{2A}AR as potential anti-inflammatory agents. The recent crystallographic analysis of A_{2A}AR agonists and antagonists in complex with the receptor provided key information on the structural determinants leading to receptor activation or blocking. In light of this, we designed a new series of 2-((4-aryl(alkyl)piperazin-1-yl)alkylamino)-5′-*N*-ethylcarboxamidoadenosines with high A_{2A}AR affinity, activation potency and selectivity obtained by merging distinctive structural elements of known agonists and antagonists of the investigated target. Docking-based SAR optimization allowed us to identify compound **42** as one of the most potent and selective A_{2A} agonist discovered so far (K_i hA_{2A}AR = 4.8 nM, EC_{50} hA_{2A}AR = 4.9 nM, K_i hA_1AR > 10000 nM, K_i hA_3AR = 1487 nM, EC_{50} hA_{2B}AR > 10000 nM).

1. Introduction

Adenosine is a well-known purine nucleoside that interacts with four G protein coupled receptors (GPCRs), named as A_1, A_{2A}, A_{2B} and A_3 adenosine receptors (ARs).[1,2] The key role of A_{2A}ARs in a variety of pathophysiological conditions, especially neurodegenerative disorders and inflammatory tissue damage, has been extensively investigated.[3-5] A_{2A}ARs are expressed in a huge array of organs including heart, liver, lung, spleen, and thymus.[4,5] In the rat brain, A_{2A}ARs are found in the striatum, nucleus accumbens, olfactory tubercle, cortex, and hippocampus, implying a role of adenosine in neuronal development, neuroprotection, and different homeostatic functions.[5,6] Moreover, high expression of A_{2A}ARs has been found in platelets, leukocytes, neutrophils, vascular smooth muscle, and endothelial cells, with important implications in the regulation of inflammatory and immune responses.[7-9]

The use of selective A_{2A} antagonists has been reported to be potentially useful in the treatment of neurodegenerative diseases such as Parkinson's disease (PD), Huntington's disease and Alzheimer's disease.[6,10-12] Istradefylline is the most advanced ligand of this class since it has been marketed as an anti-parkinsonian drug in Japan.[10,13] On the other hand, the role of AR agonists has been shown to provide a neuroprotective effect on various models of neurodegenerative disorders through the reduction of the excitatory neurotransmitter release, apoptosis and inflammatory responses.[4,6]

In the cardiovascular system, a number of A_{2A}AR agonists have been evaluated as candidate for myocardial perfusion imaging due to modulation of coronary arterial vasodilation.[3,14] Among these, Regadenoson (**5**, CV-T3146, Figure 1) was approved by FDA in 2008 and marketed by Astellas Pharma. Some studies suggest that A_{2A}AR agonists could be beneficial for the treatment of neuropathic pain being capable of modulating the production of glial cytokines.[15] The agonist BVT115959 (structure not disclosed) reached phase II studies for this indication proving tolerability and promising efficacy in diabetic patients.[4] A_{2A}AR agonists have been investigated in other

therapeutic areas such as diabetic foot ulcer, *Clostridium difficile* infection, psoriasis and atopic dermatitis.[3]

A_{2A}AR stimulation has been also shown to primarily exert anti-inflammatory effects modulating the activity of neutrophils, macrophages and T lymphocytes.[3,7] In addition, activation of A_{2A}ARs inhibits neutrophil adherence to the endothelium, degranulation of neutrophils and monocytes, and superoxide anion generation.[4] Thus, A_{2A}ARs play a key role in inflammation and selective agonists have been developed as potentially useful for the treatment of related conditions such as allergic rhinitis, asthma and chronic obstructive pulmonary disease.[3,16] Recent investigations suggested that adenosine pathway might be involved in the control of inflammation in rheumatic diseases.[8,17] Adenosine analogues could also inhibit joint destruction when used in the treatment of inflammatory articular diseases as indicated in human chondrocytes and/or synoviocytes.[18] From the cellular point of view, A_{2A} activation reduced the NF-kB pathway and diminished inflammatory cytokines such as tumor necrosis factor -α (TNF-α), interleukin 1β (IL-1β), IL-8, IL-6 and inhibited metalloproteinases-1 (MMP-1) and MMP-3 release.[19] In rheumatoid arthritis patients the stimulation of A_{2A}ARs mediated a significant decrease of pro-inflammatory cytokines and increase of IL-10 production.[20] In rat adjuvant-induced arthritis and associated pain A_{2A}AR activation was highly effective, as revealed by the marked reduction of clinical signs suggesting the potential of A_{2A}AR agonists for the pharmacological treatment of rheumatoid arthritis.[20,21] Although A_{2A} agonists, as potent vasodilators, have been associated to systemic side effects that have limited their clinical utility, it has been reported that their anti-inflammatory action is promoted by low doses unable to produce significant cardiovascular side effects.[3]

As a consequence of these encouraging results we started a research program for the identification of potent and selective A_{2A}AR agonists as new chemical agents for the treatment of inflammatory disorders by mimicking the adenosine endogenous protective system with reduced

side effects. The medicinal chemistry and clinical advancements of small-molecule modulators of the A_{2A}AR as a drug discovery target have been recently reviewed.[3]

A_{2A}AR agonists reported to date mainly reflect the nucleoside scaffold of adenosine (**1a**, Figure 1) or 5′-*N*-ethylcarboxamidoadenosine (NECA, **1b**, Figure 1). CGS21680 (**2**, Figure 1) was shown to have good binding affinity at the human (h) A_{2A}AR (K_i = 27 nM) and selectivity over the hA_{2B}AR (K_i > 10 μM) but moderate selectivity versus the hA_1AR (K_i = 290 nM) and the hA_3AR (K_i = 67 nM) subtypes.[3] Its tritiated form ([^{3}H]-CGS21680) is currently considered as the prototypical agonist radioligand for the pharmacological characterization of the A_{2A}AR. Like CGS21680, other known A_{2A}AR agonists are mostly characterized by the presence of bulky substituents at the 2-position of the adenine bicycle. In this area, King Pharmaceutical identified a series of 2-alkoxy adenosines, such as Sonedenoson (**3**, Figure 1, K_i hA_{2A}AR = 490 nM), and 2-hydrazone derivatives such as Binodenoson (**4**, K_i hA_{2A}AR = 270 nM). Regadenoson (**5**, K_i hA_{2A}AR = 290 nM), bearing a 2-*N*-pyrazolyl substitution, was later conceived by Astellas Pharma as a constrained analogue of the latter compound. In addition, a series of 4′-aza-carbocyclic nucleosides have been scrutinized as reversed amide analogs of NECA with potent A_{2A} binding potency (see compound **6**, K_i hA_{2A}AR = 5.4 nM, EC_{50} hA_1AR = 10 μM, EC_{50} hA_{2B}AR = 10 μM, EC_{50} hA_3AR = 1640 nM).[22] 2-Alkynyl NECA derivatives with sub-nanomolar affinity for the A_{2A}AR have been identified (see Apadenoson, **7**, K_i hA_{2A}AR = 0.5 nM). Pfizer laboratories investigated also the effect of N^6-substitution identifying the A_{2A} agonist UK-432097 (**8**, K_i hA_{2A}AR = 4 nM). Finally, based on a molecular modeling investigation, the histidine conjugate of CGS21680, **9** (hereinafter labeled as **J42**, K_i hA_{2A}AR = 40 nM), has been recently developed by Jacobson *et al.* as a rather potent A_{2A} agonist.[23]

For the design of new A_{2A}AR agonists, we analyzed the recent results from crystallographic investigations that provided fundamental information based on the crystal structure of known A_{2A}AR agonists (NECA and UK432097, Figure 2a) and antagonists (ZM241385, **10**, Figures 2a

and 3) bound to the receptor.[24,25] These studies confirmed a clear overlap between C^5-position of ZM241385 and the C^2-position of NECA/UK432097 in their respective binding pose at the A_{2A}AR (Figure 2a). The triazolotriazine scaffold of ZM241385 would substantially mimic the endogenous ligand lacking of the ribose moiety which is responsible for the agonist activity. The hydroxyl groups at 2′- and 3′-positions of NECA have been actually shown to establish hydrogen bond interactions with Ser277 and His278 of the binding pocket leading to receptor activation. In addition, the phenylethylamine side chain of ZM241385 seems to be in contact with F168 and I274 that are the same receptor residues surrounding C^2-position of NECA (Figure 2b,c). Thus, we speculated that the SAR profile of known A_{2A} antagonists could be exploited for the design of potent and selective agonists. In particular we focused on the structure of Preladenant (**11**, Figure 3), selected by Schering-Plough for evaluation in Phase I-III trials for the treatment of PD.[13] The pyrazolo[4,3-*e*][1,2,4]triazolo[1,5-*c*]pyrimidine (PTP) core of this compound can be considered a tricyclic analog of ZM241385 resulting from the condensation of an additional pyrazole ring. Consistent with this observation, the 7-position of Preladenant would correspond to the 5-position of ZM241385 and, accordingly, to the 2-position of NECA. A partial overlap of the binding sites of adenosine-related agonists and PTPs and their C^2 and N^7 substituents has been also suggested by Jacobson et al. in earlier docking investigations based on a rhodopsin homology model.[26]

The (substituted)phenyl-piperazino-ethyl side chain of Preladenant was the result of an intensive SAR optimization of N^7-substitution aimed at improving both A_{2A}AR affinity/selectivity and water solubility.[3] The same substitution confirmed high efficacy when introduced at the 5-position of ZM241385-related ligands.[27] In light of this, and thanks to the identification of a versatile synthetic approach which permitted us to functionalize the C^2-position of the non-selective adenosine agonist NECA, we designed a series 2-((4-aryl(alkyl)piperazin-1-yl)alkylamino)-5′-*N*-ethylcarboxamidoadenosines (general structure **17**-**43**, Figure 3). In this way, we aimed at identifying a molecular hybrid between the typical nucleoside template responsible for receptor

activation with a structural element able to warrant A_{2A} selectivity in the above cited series of bicyclic and tricyclic antagonists. In exploring the SAR of 2-substitution we first evaluated the effect of the introduction of different alkyl spacers between the piperazine ring, the adenine core and the distal phenyl ring. Moreover, with the synthesis of compounds **44-54**, the direct functionalization of the C^2-position with (substituted)arylpiperazine moieties lacking of any spacers, was investigated. Once optimized the template, with the aim of enhancing the A_{2A} affinity and selectivity through a structure based drug design (SBDD) approach, the side chain phenyl ring was substituted in specific positions.

2. Results and discussion

Chemistry. The general synthetic approach used to prepare the new 2-substituted-5′-*N* ethylcarboxamidoadenosines **17-54** is depicted in Scheme 1. 2′,3′-*O*-isopropylidene-2-chloro-5′-*N*-ethylcarboxamidoadenosine **12**[28] was treated with the appropriate [4-(substituted)phenyl(alkyl)piperazin-1-yl]alkylamines (**13a-ab**) or 1-((substituted)phenyl)piperazines (**14a-k**) resulting in the replacement of the 2-Cl group by the desired side chain. The nucleophilic displacement occurred by reacting **12** with an excess of amine in DMSO at 120 °C for 24 h. Despite the quite drastic conditions, in no case we observed a complete conversion of the starting compound that could give explanation for occasionally low reaction yields. The 2′,3′-acetonide protection of C^2-substituted nucleoside derivatives **15a-ab** and **16a-k** was removed in standard conditions by treatment with a 1:1 mixture of water and trifluoroacetic acid (4 h) at room temperature to give final compounds **17-29**, **32**, **34-42**, **44-54**. In order to obtain the final carboxylic acid derivatives **30**, **31**, **33** and **43**, a further saponification step was performed.

Most of the [4-(substituted)phenyl(alkyl)piperazin-1-yl]alkylamines (**13a-m**, **p**, **r-aa**) were prepared according to Scheme 2a in analogy with previously reported procedures.[29] Commercially available (substituted)phenyl(alkyl)piperazines (**55a-v**, **14d**) were alkylated in standard conditions

with *N*-(2-bromoethyl)phthalimide or *N*-(3-bromopropyl)phthalimide followed by the removal of the phthaloyl group by hydrazinolysis.

Butyl 2-(4-(4-(2-aminoethyl)piperazin-1-yl)phenyl)acetate **13o** and its 3-Br analogue **13ab** were prepared from ethyl 2-(4-aminophenyl)acetate (**57**) and ethyl 2-(4-amino-3-bromophenyl)acetate (**58**), respectively, as reported in scheme 2b. The 3-Br derivative **58** was obtained by bromination of **57** as previously reported.[30] Both starting reagents were firstly reacted with bis(2-chloroethyl)ethylamine in presence of K_2CO_3 and refluxed in n-butanol to afford the piperazine derivatives **59** and **60** with moderate yield.[31] Unlike previously reported, a complete transesterification of the ethyl ester group to the corresponding n-butyl ester was observed. The subsequent alkylation with *N*-Boc-2-bromoethyl-amine followed by TFA-mediated Boc deprotection, furnished the desired amines **13o** and **13ab**. The use of *N*-Boc-2-bromoethyl-amine instead of *N*-(2-bromoethyl)phthalimide allowed us to preserve the ester group from hydrazinolysis.

The ethyl 3/4-(4-(2-aminoethyl)piperazin-1-yl)benzoate derivatives **13n** and **13q** were obtained by treatment of 3/4-fluorobenzoate with an excess of piperazine[32] to give intermediates **65** and **66** that were alkylated with *N*-Boc-2-bromoethyl-amine followed by Boc removal as above described (Scheme 3a).

When not commercially available, 4-(substituted)phenyl piperazines were prepared as shown in Scheme 3b. After the selective protection of the free piperazine nitrogen of **69** by treatment with di-tert-butyldicarbonate, the phenolic group was alkylated with different (aryl)alkylhalides according to known procedures.[33] Final Boc deprotection furnished the desired compounds **14d-k.**

Lead Identification. Competition binding experiments were performed to evaluate the affinity of all the final compounds (**17-54**) for the hA_1, hA_{2A} and hA_3 ARs expressed in CHO (chinese hamster ovary) cells using as radioligands [^{3}H]-CCPA (2-chloro-N^6-cyclopentyladenosine), [^{3}H]-CGS21680 and [^{125}I]-AB-MECA (*N*^{6}-(4-Amino-3-iodobenzyl)-5′-*N*-methylcarbamoyladenosine), respectively. The compounds were also evaluated in functional assays, measuring their capability to

modulate cyclic AMP levels in CHO cells expressing hA_{2B} or hA_{2A} ARs. Structures and biological data of the synthesised compounds are listed in Tables 1-3.

In the early stage of the project we synthesized compounds **17**-**20** and **44** in order to identify the best template for further SAR optimization (see Table 1). To this aim, we evaluated the effect of the introduction of different (4-phenyl(alkyl)piperazin-1-yl)alkylamino moieties at the 2-position of NECA as in derivatives **17**-**20**. In this subset of molecules, linear alkyl(amino) spacers of variable length have been introduced between the piperazine nucleus, the distal phenyl ring and the adenine bicycle. With compound **44** the effect of the removal of any alkyl(amino) spacer has been investigated as well.

The 2-[2-(4-phenyl-piperazin-1-yl)-ethylamino] derivative **17** was first evaluated as a direct analogue of Preladenant (see structure **11**, Figure 3) and it was shown to bind A_{2A}AR with a K_i value of 55 nM and good selectivity over A_1 and A_3AR subtypes (K_i > 10000 and = 2161 nM, respectively). While a negligible activity of **17** at the A_{2B}AR was observed, a promising behaviour of full agonist toward A_{2A}AR was highlighted by the functional assay with an EC_{50} value in the nanomolar range (EC_{50} hA_{2A}AR 91 nM). The homologue **18** displayed a 4/5-fold decrease of A_{2A}AR affinity (K_i hA_{2A}AR = 237 nM) and potency (EC_{50} hA_{2A}AR = 438 nM), thus a proximal ethylamino spacer was maintained in following derivatives. In the same way, substitution of the phenyl ring of **17** with a benzyl (see compound **19**) or a phenethyl (see compound **20**) moiety determined a marked decrease of A_{2A}AR affinity (K_i hA_{2A}AR = 659 and 967 nM, respectively) indicating an unfavourable effect of a distal methylene or ethylene spacer. Finally, the loss of A_{2A}AR affinity of compound **44** clearly indicated the importance of an alkylamino spacer in the proximal portion of the C^2-side chain.

These results supported our hypothesis regarding the possible correspondence between the 7-substitution of PTPs and 2-substitution of NECA-related nucleosides, thereby **17** was selected for the development of more potent and selective A_{2A} agonists.

Binding mode of 17 and hints for drug design. Molecular modelling techniques can be instrumental in deciphering the structural basis underlying the binding affinity of a compound to its target protein.[34-37] Moreover, computational techniques (i.e docking and molecular dynamics (MD) simulations) can pave the way for the design of new ligands with increased affinity for their protein target and, most importantly, improved selectivity towards off-target proteins. In this regards, we embarked in the elucidation of the structural details underlying the binding mode of compound **17** in the A_{2A} receptor structure, which was the most promising candidate in the initial stage of the design of new A_{2A} agonists (see Table 1). By means of docking and MD studies the binding mode of **17** within the A_{2A}AR binding site, depicted in Figure 4a, was obtained.

In the predicted complex, the ligand adenosine core is adapted in a similar fashion to that observed in the X-ray crystal structure of the A_{2A} receptor in complex with the agonists NECA and UK432097 (See Supplementary Figure S1).[25,38] Key interactions are: (*i*) H-bonds between the sugar moiety and T88, H250, S277, and H278 residues; (*ii*) a ionic interaction between the positively charged nitrogen on the piperazinyl ring and E169 residue on the extracellular loop 2 (ECL2); (*iii*) hydrophobic interaction with L167, W246, L267, M270, and Y271 residues; (*iv*) a π-stacking interaction between F168 residue and the adenosine ring; and (*v*) a cation-π interaction between the terminal phenyl ring and K153. The selected binding mode was also highly stable during a 100 ns long MD simulations, showing small root-mean squared deviations (rmsd) calculated on the ligand heavy atoms (Figure 4b) with respect to the binding mode reported in Figure 4a.

The resulting binding mode was also helpful when attempting to explain the activity profile of **17** towards the other ARs. Indeed, the ligand electron-rich phenyl ring accommodates in a region lined by hydrophobic residues (L167, L267, M270, and Y271), which in turn reinforce the cation-π interaction with K153 (Figure 4a). Moreover, sequence alignment and homology models of the A_1, A_{2B}, and A_3 ARs (Insets in Figure 4a) supports the notion that the residues in the A_{2A}-ECL2 domain (cyan transparent cartoon in the Figure 4a insets), together with Y271, are responsible for

the selectivity profile showed by **17** (See Table 1). Indeed, the A_1AR, A_{2B}AR and A_3AR, receptors do not possess any positively charged residues in the ECL2 region, and the same position (K153) is occupied by Trp, Thr and Tyr residues, respectively. These latter residues being shorter and less flexible than the A_2AR Lys side chain should not be able to establish relevant interactions with the phenyl ring of **17** (Insets in Figure 4a), thereby explaining the reduced affinity profile of **17** towards A_1AR, A_{2B}AR, and A_3AR. This observation is also supported by the comparison of the binding mode of the most selective compound reported by Jacobson *et al.*[23] (**J42**, Figure 1), and **17** (Figure 4c). Indeed, also **J42** interacts with K153 through its D-His moiety (Figure 4c).

Prompted by these observations, we also analysed the conformational behaviour of the phenyl ring along the MD simulations (Figure 5a). In this case the phenyl group of **17** is endowed with great flexibility around the α dihedral angle (Figure 5a) and in principle the introduction of small substituents at 2′ position of the phenyl ring could improve the affinity profile of **17** for the A_{2A}AR by reducing the degree of freedom of **17** along the α dihedral angle thereby stabilizing the putative bioactive conformation. This hypothesis was also supported by the comparison of the QM energy scan for the α dihedral angles of **17** and for the same compounds carrying a fluorine atom at 2′ position (**17-F,** Figure 5b). Indeed, the presence of the fluorine atom greatly increases the energy barrier between the different rotamers of α. **17-F** displays an energetic minimum around 300°, which is perfectly superimposable to the conformer of **17** in the reported theoretical binding mode (Figure 5 and inset in Figure 5b). Therefore, with the aim of increasing the interaction of **17** with ECL2, and to enhance its selectivity profile, substitutions on 2′, 3′ and 4′ positions of the phenyl ring were considered.

SAR Optimization. On the basis of the structural hints obtained through the molecular modelling studies, a set of substitutions were introduced at the terminal phenyl ring of **17** and their effect in terms of binding and functional parameters have been reported in Table 2. The non-

selective ARs agonist NECA and the prototypical A_{2A} agonist CGS21680 were integrated in both binding and functional assays as internal references.

Most of the newly examined compounds showed marked affinity for the A_{2A}AR with K_i values ranging from 4.8 to 277 nM. Moreover, outstanding selectivity over the A_1AR (K_i hA_1AR > 10000 nM) and good selectivity versus the A_3AR (K_i hA_3AR from 759 to 10000 nM) were observed. In addition, compounds **17**-**43** were all devoid of any agonist activity at the A_{2B}AR up to 10 μM.

In compounds **21**-**31** the monosubstitution of the 4-position with electron withdrawing or donating groups was investigated. Among the 4-halogenated derivatives **21**-**24**, a 4-Cl (**22**) or a 4-Br (**23**) determined a 2-fold enhancement of A_{2A}AR affinity (K_i hA_{2A}AR = 25 and 29 nM, respectively) if compared to the unsubstituted parent compound **17**. A 4-F (**21**) or a 4-I (**24**) group had an opposite effect with almost a 2-fold decrease of affinity (K_i hA_{2A}AR = 98 and 92 nM, respectively). Thus an electron-withdrawing group of the proper size at this position seems to be preferred. Indeed, the bulkier 4-CF_3 (**25**) proved to be less beneficial with a smaller increase of A_{2A} affinity (K_i hA_{2A}AR = 36). A stronger electron withdrawing group such as 4-NO_2 (**26**), was shown to be as effective as 4-Cl substitution for A_{2A} affinity (K_i hA_{2A}AR = 24 nM and EC_{50} hA_{2A}AR = 36 nM) but significantly detrimental for selectivity over the A_3AR (K_i hA_3AR/ K_i hA_{2A}AR of 32 and 67 for compounds **26** and **22**, respectively). A weak electron donating methyl function at the 4-position had a slight negative effect on A_{2A} affinity of **27** (K_i = 88 nM), while stronger electron donating group such as 4-OCH_3 and 4-$OCH_2CH_2OCH_3$ (introduced in analogy with Preladenant) resulted in compounds **28** and **29** nearly equipotent to the unsubstituted **17**. A carboxylic (**30**) and an acetic (**31**) functional group were also investigated for their potential ability to establish favourable ionic interactions with the K153 receptor residue, and 4-COOH proved to be particularly effective in enhancing A_{2A} vs A_3 selectivity (K_i hA_{2A}AR = 30 nM; K_i hA_3AR/K_i hA_{2A}AR = 194).

In compounds **32** and **33** the preferred substitutions at the 4-position (4-Cl and 4-COOH) were moved to the meta position revealing a substantial maintenance or a slight worsening of the

pharmacological profile if compared to the closely related **22** and **30**. The *ortho*-substitution of the phenyl ring (see **34**-**37**) resulted occasionally more effective in improving A_{2A} affinity. In particular, moving the fluorine atom from *para*- to *ortho*-position resulted in a 12-fold increase of A_{2A} affinity and potency (compare **21** to **34**), in agreement with our computational predictions, where substituents in the 2′-position can stabilize the putative ligand bioactive conformation. Interestingly, this data are also strongly in agreement with the SAR studies regarding the 5-substitution of ZM241385-related A_{2A}AR antagonists with analogous side chains[27] and this further contributed to validate the rational approach of the project here reported. Bulkier (CF_3, **36**) and/or electron-donating (OCH_3, **37**) groups at the same position were significantly less tolerated.

Finally, the effect of disubstitution was probed in compounds **38**-**43**. When a 3-Cl was combined to a 4-F (**38**, K_i $hA_{2A}AR$ = 34 nM), a 4-Cl (**39**, K_i $hA_{2A}AR$ = 26 nM) or a 5-Cl (**40**, K_i $hA_{2A}AR$ = 33 nM) we observed a general preservation of the binding properties in comparison with the monosubstituted **32** (K_i $hA_{2A}AR$ = 23 nM). On the other hand, combining the 2-F substitution with a 3-F (**41**, K_i $hA_{2A}AR$ = 5.5 nM, EC_{50} $hA_{2A}AR$ = 10.2 nM, K_i hA_3AR/ K_i $hA_{2A}AR$ = 330) or a 4-Cl (**42**, K_i $hA_{2A}AR$ = 4.8 nM, EC_{50} $hA_{2A}AR$ = 4.9 nM, K_i hA_3AR/ K_i $hA_{2A}AR$ = 310), we identified the most potent and selective A_{2A} agonists of the whole series. Interestingly, compound **42** was the result of the combination of the best performing monosubstitutions at the ortho and para positions, suggesting possible synergistic interactions with the investigated receptor.

In compound **43**, a 2-Br substitution was combined with a 4-CH_2COOH chain. This molecule was prepared as suggested by predictive docking studies of substituted analogs of **17**. Also in this case, the acetic function was supposed to engage a salt bridge with K153, on the other hand the bromine atom seemed to disfavour a co-planar conformation of the phenyl-piperazine moiety, orientating the acidic function toward the K153 residue. In agreement with our computational predictions, compound **43** showed a 2-fold increase of A_{2A}AR affinity and almost a 4-fold increase of A_{2A} *vs* A_3AR selectivity if compared to the unsubstituted congener **17**. Furthermore, the

comparison between **43** and the monosubstituted analogue **31** confirmed the importance of the 2-substitution as a significant enhancement of both A_{2A} affinity and selectivity was observed.

Despite the lack of affinity of compound **44** (Table 1), we decided to further explore the potential of such a template performing some substitutions at the phenyl ring with the aim to restore the biological activity and obtain additional SAR information. As a result, we prepared the small series of NECA-related nucleosides listed in Table 3 (**44**-**54**). As emerging from the biological data, 4-F substitution (see compound **45**) did not exert variation of the binding profile. Quite unexpectedly, a 4-OCH_3 group (see compound **46**) induced good A_3AR affinity (K_i hA_3AR = 70 nM) and selectivity (about 143-fold over the remaining AR subtypes). This datum is clearly in disagreement with the SAR profile of the ligands reported in Table 2 suggesting a totally different binding mode for nucleoside derivatives deprived of the proximal ethylamine spacer. Prompted by the profile of compound **46**, we introduced different alkoxy groups (**47**-**54**) that however led to AR agonists with variable selectivity profiles. The 4-$OCH_2CH_2OCH_3$ substitution, mimicking preladenant, led to compound **47** that was a weak A_1/A_3AR dual ligand (K_i hA_1AR = 147 nM, K_i hA_3AR = 293 nM). Among the (4-substituted)benzyloxy derivatives **48**-**51**, we identified potent but poorly selective AR agonists in which the 4-CF_3 derivative **51** distinguished for its high affinity for the A_1AR subtype (K_i hA_1AR = 4.5 nM). A OCH_2(4-pyridyl) moiety (**52**) was poorly tolerated by the A_1, A_{2A} and A_{2B}AR subtypes, while a low affinity for the A_3AR was observed (K_i hA_3AR = 248 nM). The non-selective profile of **53** and **54** further suggested that the 2-arylpiperazine side chain would promote non-specific interactions with most of the AR subtypes. None of the synthesized molecules showed significant binding selectivity for the A_{2A}AR and the pairwise comparison of **45**-**47** with their analogues **21**, **28** and **29** in Table 2, clearly indicated the fundamental importance of the proximal ethylamine linker to ensure favorable interactions with the investigated target.

Functional Assays: hA_{2B} and hA_{2A} ARs. As mentioned above, most of the compounds reported in Tables 1-3 were basically inactive at the hA_{2B} AR subtype with EC_{50} > 10 μM. Few exceptions are represented by 4-(substituted)arylpiperazine derivatives in Table 3 among which **53** exerted high nanomolar hA_{2B} activity (EC_{50} = 389). Most importantly, the investigated compounds behave as full hA_{2A}AR agonists in the cAMP functional assay as depicted in figure 6B. Interestingly, binding data for each ligand reflected in a correlated A_{2A} agonist potency with K_i and EC_{50} values in the same nanomolar range (compare figure 6A and 6B). Thus, the molecules showing the best affinities for hA_{2A}AR confirmed to display high potency in the functional assay (see **34**, **35**, **41** and **42**). Derivative **42**, with the highest hA_{2A} affinity (K_i = 4.8 nM), also emerged as the most potent compound of the series with an EC_{50} value of 4.9 nM.

3. Conclusion

In conclusion, we herein reported our preliminary results from a research program aimed at identifying potent and selective agonists of the A_{2A}AR. The design approach was based on the crystallographic analysis recently performed on A_{2A}AR ligands in complex with the receptor.[24,25] These studies allowed us to extrapolate useful information about the structural determinants leading to selective receptor activation/blocking. In particular, the superimposition of prototypical A_{2A}AR agonists (i.e. NECA) and antagonists (i.e. ZM241385) bound to the receptor suggested overlaps of critical positions in view of which we have been successful in conferring very high A_{2A} affinity, selectivity and potency in a series of adenosine-based ligands. These compounds have been functionalized at the 2-position of the adenine core with side chains arising from the medicinal chemistry of known A_{2A} antagonists confirming the possibility to merge distinctive structural elements that characterize agonists and antagonists for the construction of useful "molecular hybrids". Docking-based SAR optimization guided us to identify compound **42** as one of the most

potent and selective A_{2A} agonist discovered so far (K_i $hA_{2A}AR$ = 4.8 nM, EC_{50} $hA_{2A}AR$ = 4.9 nM, K_i hA_1AR > 10000 nM, K_i hA_3AR = 1487 nM, EC_{50} $hA_{2B}AR$ > 10000 nM).

4. Experimental section

4.1. Chemistry

Chemical Materials and Methods. Reaction progress and product mixtures were monitored by thin-layer chromatography (TLC) on silica gel (precoated F_{254} Macherey-Nagel plates) and visualized by UV lamp (254 nm light source). The organic solutions from extractions were dried over anhydrous sodium sulfate. Chromatography was performed on Merck 230-400 mesh silica gel. ^{1}H-NMR data were determined in $CDCl_3$ or DMSO-d_6 solutions with a Varian VXR 200 spectrometer or a Varian Mercury Plus 400 spectrometer. Peak positions are given in parts per million (δ) downfield from tetramethylsilane as internal standard, and J values are given in hertz. Splitting patterns are designed as s, singlet; d, doublet; t, triplet; q, quartet; m, multiplet; b, broad. Melting points for purified products were determined in a glass capillary on a Stuart Scientific electrothermal apparatus SMP3 and are uncorrected. Electrospray ionization mass spectrometry (ESI/MS) was performed with an Agilent 1100 Series LC/MSD in positive scan mode using direct injection of the purified compound solution (MH^+). Elemental analyses were performed by the microanalytical laboratory of Dipartimento di Chimica, University of Ferrara, and were within ± 0.4% of the theoretical values for C, H, and N. All final compounds revealed a purity of not less than 95%. When not commercially available, 4-(substituted)phenyl(alkyl)piperazin-1-yl)alkylamines **13a-ab** and 1-((substituted)phenyl)piperazines **14a-k** were prepared as described in the supporting information.

General procedure for the preparation of (3a*S*,4*S*,6*R*,6a*R*)-6-(6-amino-2-(substituted)-9*H*-purin-9-yl)-*N*-ethyl-2,2-dimethyltetrahydrofuro[3,4-*d*][1,3]dioxole-4-carboxamides 15a-ab and 16a-k.

A mixture of the protected 2-Cl-NECA derivative **12** (230 mg, 0.6 mmol), the appropriate [4-(substituted)phenyl(alkyl)piperazin-1-yl]alkylamines (**13a-ab**, 1.2 mmol) or 1-((substituted)phenyl)piperazines (**14a-k**, 1.2 mmol) and TEA (250 µL, 1.8 mmol) in DMSO (500 µl) was stirred at 120 °C for 24 h in a schlenk tube. The solvent was evaporated and the residue partitioned between H_2O (20 mL) and EtOAc (20 mL). After separation, the aqueous phase was further extracted with EtOAc (3x30 mL) and the combined organic layers were dried over anhydrous Na_2SO_4, filtered and the solvent evaporated to give a residue which was purified by flash chromatography using as eluent an appropriate mixture of EtOAc and MeOH.

(3a*S*,4*S*,6*R*,6a*R*)-6-(6-amino-2-((2-(4-phenylpiperazin-1-yl)ethyl)amino)-9*H*-purin-9-yl)-*N*-ethyl-2,2-dimethyltetrahydrofuro[3,4-*d*][1,3]dioxole-4-carboxamide (15a)

White solid; $C_{27}H_{37}N_9O_4$; 35% yield; mp 142 °C. ^{1}H NMR (200 MHz, $CDCl_3$) δ (ppm) 0.65 (t, *J* = 7.4 Hz, 3H), 1.42 (s, 3H), 1.59 (s, 3H), 1.98-2.21 (m, 6H), 2.68-2.88 (m, 2H), 3.43-3.51 (m, 4H), 3.59-3.68 (m, 2H), 4.60-4.65 (m, 1H), 5.42-5.61 (m, 4H), 6.01-6.18 (m, 2H), 6.90-6.97 (m, 3H), 7.21-7.25 (m, 3H), 7.62 (s, 1H); MS (ESI): $[MH]^+$ = 553.63.

(3a*S*,4*S*,6*R*,6a*R*)-6-(6-amino-2-((3-(4-phenylpiperazin-1-yl)propyl)amino)-9*H*-purin-9-yl)-*N*-ethyl-2,2-dimethyltetrahydrofuro[3,4-*d*][1,3]dioxole-4-carboxamide (**15b**)

White solid; $C_{28}H_{39}N_9O_4$; 22% yield; mp 170 °C. ^{1}H NMR (200 MHz, $CDCl_3$) δ (ppm) 0.66 (t, *J* = 7.4 Hz, 3H), 1.38 (s, 3H), 1.58 (s, 3H), 1.98-2.21 (m, 6H), 2.85-3.18 (m, 6H), 3.35-3.51 (m, 4H), 4.60-4.65 (m, 1H), 5.35-5.55 (m, 3H), 5.57-5.61 (m, 1H), 5.89 (bt, *J* = 5.2 Hz, 1H), 6.03 (s, 1H), 6.90-6.95 (m, 3H), 7.20-7.24 (m, 3H), 7.53 (s, 1H); MS (ESI): $[MH]^+$ = 567.52.

(3a*S*,4*S*,6*R*,6a*R*)-6-(6-amino-2-((2-(4-benzylpiperazin-1-yl)ethyl)amino)-9*H*-purin-9-yl)-*N*-ethyl-2,2-dimethyltetrahydrofuro[3,4-*d*][1,3]dioxole-4-carboxamide (**15c**)

White solid; $C_{28}H_{39}N_9O_4$; 44% yield; mp 102-104 °C. ^{1}H NMR (200 MHz, DMSO-d_6) δ (ppm) 0.55 (t, *J* = 7.2 Hz, 3H), 1.31 (s, 3H), 1.49 (s, 3H), 2.24-2.45 (m, 8H), 2.61-2.93 (m, 2H), 3.15-3.21 (m,

2H), 3.35-3.39 (m, 2H), 3.45 (s, 2H), 4.45 (d, *J* = 1.8 Hz, 1H), 5.38-5.55 (m, 2H), 5.96 (bt, *J* = 5.4 Hz, 1H), 6.22 (s, 1H), 6.69 (bs, 2H), 7.12 (bt, *J* = 7.6 Hz, 1H), 7.21-7.39 (m, 5H), 7.82 (s, 1H); MS (ESI): $[MH]^+$ = 566.53.

(3a*S*,4*S*,6*R*,6a*R*)-6-(6-amino-2-((2-(4-phenethylpiperazin-1-yl)ethyl)amino)-9*H*-purin-9-yl)-*N*-ethyl-2,2-dimethyltetrahydrofuro[3,4-*d*][1,3]dioxole-4-carboxamide (**15d**)

Pale yellow solid; $C_{29}H_{41}N_9O_4$; 57% yield; mp 167-169 °C. ^{1}H NMR (200 MHz, DMSO-d_6) δ (ppm) 0.56 (t, *J* = 7.2 Hz, 3H), 1.34 (s, 3H), 1.51 (s, 3H), 2.31-2.46 (m, 8H), 2.67-2.99 (m, 6H), 3.17-3.24 (m, 2H), 3.39-3.42 (m, 2H), 4.47 (d, *J* = 1.6 Hz, 1H), 5.39-5.57 (m, 2H), 5.97 (bt, *J* = 5.4 Hz, 1H), 6.23 (s, 1H), 6.70 (bs, 2H), 7.14-7.27 (m, 6H), 7.83 (s, 1H); MS (ESI): $[MH]^+$ = 580.65.

(3a*R*,4*S*,6*R*,6a*S*)-6-(6-amino-2-(4-phenylpiperazin-1-yl)-9*H*-purin-9-yl)-*N*-ethyl-2,2-dimethyl-tetrahydrofuro[3,4-*d*][1,3]dioxole-4-carboxamide (16a)

White solid; $C_{25}H_{32}N_8O_4$; 56% yield; mp 153-154 °C. ^{1}H-NMR (200 MHz, $CDCl_3$): δ (ppm) 0.70 (t, *J* = 7.2 Hz, 3H), 1.41 (s, 3H), 1.60 (s, 3H), 2.81-3.04 (m, 2H), 3.22-3.33 (m, 4H), 3.82-3.97 (m, 4H), 4.67 (d, *J* =1.4, 1H), 5.50-5.62 (m, 2H), 5.83 (bt, *J* = 5.4 Hz, 1H), 6.06 (d, *J* = 0.8, 1H), 6.82-7.05 (m, 3H), 7.29-7.36 (m, 4H), 7.57 (s, 1H); MS (ESI): $[MH]^+$ = 509.20.

(3a*R*,4*S*,6*R*,6a*S*)-6-(6-amino-2-(4-(4-fluorophenyl)piperazin-1-yl)-9*H*-purin-9-yl)-*N*-ethyl-2,2-dimethyl-tetrahydrofuro[3,4-*d*][1,3]dioxole-4-carboxamide (16b)

White solid; $C_{25}H_{31}FN_8O_4$; 72 % yield; mp 232 °C. ^{1}HNMR (200 MHz DMSO-d_6) δ 0.55 (t, *J* = 7.4 Hz, 3H), 1.35 (s, 3H), 1.52 (s, 3H), 2.61-2.97 (m, 2H), 3.02-3.19 (m, 4H), 3.65-3.84 (m, 4H), 4.51 (d, *J* = 1.2 Hz, 1H), 5.42-5.57 (m, 2H), 6.27 (s, 1H), 6.89 (bs, 2H), 7.03-7.18 (m, 4H), 7.21 (bt, *J* = 7.6 Hz, 1H), 7.90 (s, 1H); MS (ESI): $[MH]^+$ = 527.30.

General procedure for the preparation of (2*S*,3*S*,4*R*,5*R*)-5-(6-amino-2-(substituted)-9*H*-purin-9-yl)-*N*-ethyl-3,4-dihydroxytetrahydrofuran-2-carboxamides 17-54.

The isopropylidene derivatives **15a-ab** and **16a-k** (0.2 mmol) were dissolved in a 1:1 mixture of TFA and water (6 mL) and the solution was stirred at room temperature for 4 h. The solvents were

evaporated under reduced pressure to give a residue which was suspended with a saturated $NaHCO_3$ aqueous solution and extracted with EtOAc (3x20 mL). The combined organic layers were dried over Na_2SO_4, filtered and the solvent evaporated under vacuum to give a residue that was purified by flash chromatography using as eluent an appropriate mixture of EtOAc and MeOH and affording the final compounds **17-29**, **32**, **34-42**, **44-54**. In order to obtain the final carboxylic acid derivatives **30**, **31**, **33** and **43**, the residue after evaporation was instead dissolved in a mixture of NaOH aqueous solution (5%, 5 mL) and MeOH (5 mL) and stirred at room temperature for 1 h. After concentration of the methanolic fraction, the mixture was neutralized with HCl (5%), extracted with EtOAc (5x10 mL) then the solvent was dried over Na_2SO_4, filtered and evaporated to give a residue that was purified by flash chromatography using as eluent a mixture of $CHCl_3$ and MeOH 7:3.

(2*S*,3*S*,4*R*,5*R*)-5-(6-amino-2-((2-(4-phenylpiperazin-1-yl)ethyl)amino)-9*H*-purin-9-yl)-*N*-ethyl-3,4-dihydroxytetrahydrofuran-2-carboxamide (17)

White solid; 58% yield; mp 164-165 °C. ^{1}H NMR (400 MHz, DMSO-d_6) δ (ppm) 1.01 (t, J = 7.6 Hz, 3H), 2.51-2.60 (m, 4H), 3.10-3.13 (m, 4H), 3.14-3.18 (m, 2H), 3.20-3.28 (m, 1H), 3.36-3.45 (m, 3H), 4.14-4.19 (m, 1H), 4.25 (d, J = 2.0 Hz, 1H), 4.65-4.75 (m, 1H), 5.50-5.58 (m, 1H), 5.63-5.67 (m, 1H), 5.83 (d, J = 6.8 Hz, 1H), 5.96 (bt, J = 5.4 Hz, 1H), 6.76 (m, 1H), 6.83 (bs, 2H), 6.90-6.94 (m, 2H), 7.18-7.22 (m, 2H), 8.01 (s, 1H), 8.16 (bt, J = 7.6 Hz, 1H); MS (ESI): $[MH]^+$ = 512.27. Anal. Calcd for ($C_{24}H_{33}N_9O_4$) C, 56.35; H, 6.50; N, 24.64. Found: C, 56.29 ; H, 6.48; N, 24.72.

(2*S*,3*S*,4*R*,5*R*)-5-(6-amino-2-((3-(4-phenylpiperazin-1-yl)propyl)amino)-9*H*-purin-9-yl)-*N*-ethyl-3,4-dihydroxytetrahydrofuran-2-carboxamide (18)

White solid; 54% yield; mp 165-166 °C. ^{1}H NMR (400 MHz, DMSO-d_6) δ (ppm) 1.01 (t, J = 7.6 Hz, 3H), 1.65-1.79 (m, 2H), 2.32-2.43 (m, 2H), 2.45-2.49 (m, 4H), 3.08-3.17 (m, 4H), 3.20-3.39 (m, 4H), 4.16-4.21 (m, 1H), 4.25 (d, J = 2.0 Hz, 1H), 4.65-4.73 (m, 1H), 5.50 (d, J = 6.4 Hz, 1H),

5.60 (d, *J* = 4.0 Hz, 1H), 5.83 (d, *J* = 6.8 Hz, 1H), 6.26 (bt, *J* = 5.4 Hz,1H), 6.74-6.78 (m, 3H), 6.86-6.95 (m, 2H), 7.15-7.28 (m, 2H), 8.01 (s, 1H), 8.07 (bt, *J* = 7.6 Hz, 1H); MS (ESI): $[MH]^+$ = 526.31. Anal. Calcd for ($C_{25}H_{35}N_9O_4$) C, 57.13; H, 6.71; N, 23.98. Found: C, 57.24; H, 6.78; N, 23.87.

(2*S*,3*S*,4*R*,5*R*)-5-(6-amino-2-((2-(4-benzylpiperazin-1-yl)ethyl)amino)-9*H*-purin-9-yl)-*N*-ethyl-3,4-dihydroxytetrahydrofuran-2-carboxamide (19)

White solid; 48% yield; mp 116-117 °C. ^{1}H NMR (200 MHz, DMSO-d_6) δ (ppm) 1.01 (t, *J* = 6.8 Hz, 3H), 2.23-2.40 (m, 6H), 3.05-3.29 (m, 4H), 3.34-3.41 (m, 4H), 3.46 (s, 2H), 4.12-4.19 (m, 1H), 4.24 (d, *J* = 2.0 Hz, 1H), 4.62-4.75 (m, 1H), 5.48 (d, *J* = 6.0 Hz, 1H), 5.59 (d, *J* = 4.0 Hz, 1H), 5.82 (d, *J* = 7.0 Hz, 1H), 5.92 (bt, *J* = 5.6 Hz, 1H), 6.83 (bs, 2H), 7.18-7.39 (m, 5H), 8.00 (s, 1H), 8.15 (bt, *J* = 7.6 Hz, 1H); MS (ESI): $[MH]^+$ = 526.53. Anal. Calcd for ($C_{25}H_{35}N_9O_4$) C, 57.13; H, 6.71; N, 23.98. Found: C, 57.25; H, 6.79; N, 23.83.

(2*S*,3*S*,4*R*,5*R*)-5-(6-amino-2-((2-(4-phenethylpiperazin-1-yl)ethyl)amino)-9*H*-purin-9-yl)-*N*-ethyl-3,4-dihydroxytetrahydrofuran-2-carboxamide (20)

White solid; 55% yield; mp 167-168 °C. ^{1}H NMR (200 MHz, DMSO-d_6) δ (ppm) 1.02 (t, *J* = 7.2 Hz, 3H), 2.31-2.49 (m, 8H), 2.68-2.76 (m, 2H), 3.03-3.24 (m, 4H), 3.39-3.61 (m, 4H), 4.13-4.21 (m, 1H), 4.25 (d, *J* = 1.6 Hz, 1H), 4.63-4.72 (m, 1H), 5.49 (d, *J* = 6.4 Hz, 1H), 5.60 (d, *J* = 4.0 Hz, 1H), 5.82 (d, *J* = 7.4 Hz, 1H), 5.87 (bt, *J* = 5.4 Hz, 1H), 6.83 (bs, 2H), 7.16-7.31 (m, 5H), 8.00 (s, 1H), 8.16 (bt, *J* = 7.6 Hz, 1H); MS (ESI): $[MH]^+$ = 540.40. Anal. Calcd for ($C_{26}H_{37}N_9O_4$) C, 57.87; H, 6.91; N, 23.36. Found: C, 57.95; H, 6.78; N, 23.45.

(2*S*,3*S*,4*R*,5*R*)-5-(6-amino-2-(4-phenylpiperazin-1-yl)-9*H*-purin-9-yl)-*N*-ethyl-3,4-dihydroxytetrahydrofuran-2-carboxamide (44)

Pale white solid; 47% yield; mp 123-124 °C. ^{1}HNMR (200 MHz DMSO-d_6) δ 1.00 (t, *J* = 7.4 Hz, 3H), 3.08-3.21 (m, 6H), 3.77-3.83 (m, 4H), 4.20-4.28 (m, 2H), 4.65-4.71 (m, 1H), 5.53 (d, *J* = 6.2 Hz, 1H), 5.61 (d, *J* = 4.6 Hz, 1H), 5.90 (d, *J* = 7.0 Hz, 1H), 6.77-6.84 (m, 1H), 6.90-7.01 (m, 4H),

7.19-7.27 (m, 2H), 7.93 (bt, *J* = 7.6 Hz, 1H), 8.12 (s, 1H); MS (ESI): $[MH]^+$ = 469.20. Anal. Calcd for ($C_{22}H_{28}N_8O_4$) C, 56.40; H, 6.02; N, 23.92. Found: C, 56.25; H, 6.15; N, 23.77.

(2*S*,3*S*,4*R*,5*R*)-5-(6-amino-2-(4-(4-fluorophenyl)piperazin-1-yl)-9*H*-purin-9-yl)-*N*-ethyl-3,4-dihydroxytetrahydrofuran-2-carboxamide (45)

White solid; 59% yield; mp 159 °C. ^{1}HNMR (200 MHz DMSO-d_6) δ 1.00 (t, *J* = 7.4 Hz, 3H), 3.00-3.20 (m, 6H), 3.77-3.84 (m, 4H), 4.20-4.28 (m, 2H), 4.64-4.69 (m, 1H), 5.51 (d, *J* = 6.4 Hz, 1H), 5.59 (d, *J* = 4.6 Hz, 1H), 5.89 (d, *J* = 6.8 Hz, 1H), 6.90-7.11 (m, 6H), 7.92 (bt, *J* = 7.6 Hz, 1H), 8.12 (s, 1H); MS (ESI): $[MH]^+$ = 487.10. Anal. Calcd for ($C_{22}H_{27}FN_8O_4$) C, 54.31; H, 5.59; N, 23.03. Found: C, 54.21; H, 5.48; N, 23.23.

4.2. Molecular Modelling

A_{2A} X-ray selection and structure refinement. Twelve A_{2A} X-ray crystal structures were solved so far. Among them, 2YDV[25] and 3QAK[38] are the best candidate structures to perform docking studies of **17** a new A_{2A} agonist. The comparison of 2YDV and 3QAK X-ray structures (See Supplementary Figure S2) reveals important conformational changes at TM6-ECL3-TM7 level. In this regards 3QAK seems to be the X-ray structure of choice, because of the similarity of the co-crystallized ligand (UK432097, Supplementary Figure S2) and the shape of the orthosteric binding pocket. Unfortunately, in 3QAK structure the ECL2 domain is not completely solved, as in the case of the 2YDV structure (Supplementary Figure S2). Therefore, we decided to merge the ECL2 structure of 2YDV with the 3QAK X-ray structure (Supplementary Figure S2). The creation of this hybrid structure (2YDV-3QAK) was dictated by the fact that most probably in the ECL2 several sequence differences between the different ARs might be exploited to achieve selectivity amongst the different subtypes (Supplementary Figure S3). This hypothesis is also supported by the work of Jacobson *et al.*,[23] showing that ligands able to interact with lysine residues located on ECL2 (Supplementary Figure S2), show some degree of selectivity toward A_{2A} receptor.

The obtained A_{2A} 3D structure was submitted to a loop refinement process using Prime,[39] and the refined protein structure was minimized using OPLSA2005 as force field, the PRCG methods until a gradient of 0.001 kcal/mol*Å^2 applying a stepwise relaxation protocol for which harmonic constraints were progressively reduced for backbone and side chains.

Docking Studies. The refined A_{2A} receptor was used to carry out docking studies. **17** and **J42** were built using the fragment builder tool of Maestro9.1.[39] The compounds were geometrically optimized by means of Macromodel, using MMFFs as force field, water as implicit solvent until a convergence value of 0.05kcal/mol*Å^2. The computational protocol applied consists of the application of 500 steps of the Polak-Ribiére conjugate gradient (PRCG) for structure minimizations. The A_{2A} protein structure was prepared through the Protein Preparation Wizard of the Maestro9.1.[39] Docking was accomplished through the Glide tool available in Maestro9.1. The grid was centred on the residues shaping the UK432097 binding pocket defined by the E169, L167, F168, T88, W246, H250, L267, M270, Y271, S277, and H278 (according to the protein full length numbering scheme). Each docking run was carried out with the standard precision (SP) method, and the van deer Waals scaling factor of non polar atoms was set to 0.8. Twenty docking poses were obtained and among these poses we selected the best pose in accordance to (i) the Glide scoring function and that (ii) showing the lowest rmsd of the adenosine core, with respect to that in the UK432097 X-ray crystal structure. The selected docking pose were minimized using OPLSA2005 as force field, the PRCG methods until a gradient of 0.001 kcal/mol*Å^2 applying a stepwise relaxation protocol for which harmonic constraints were progressively reduced for backbone, side chains and ligand atoms.

Molecular Dynamics Simulations. The refined A_{2A}-**17** complex was embedded in an explicit POPC/Cholesterol (2:1) bilayer, applying a protocol earlier described.[40-42] The first N-terminal (I3) and the last C-terminal (L308) residues were capped with ACE and NME respectively.

Molecular dynamics (MD) simulations of the A_{2A}-**17** complex, embedded in the explicit POPC/Cholesterol (2:1) bilayer were performed using NAMD2.9 MD simulations software[43,44] and using the Amber99*SBildn* and lipid11 as force field.[45] **17** atomic single charges were computed using Gaussian03, HF/6-31** as theory level,[46] and fitted with restrained electrostatic potential (RESP). Atom type and parameters for **17** were retrieved from gaff.[45]

Computational and structural details about the generation of the A_{2A}-**17**/membrane complex and MD simulations setting are deeply discussed in Supplemental Material.

QM energy scan. The Jaguar tool within Schroedinger software suite 9.1[39] was used to perform a geometry scan for compounds **17**, and the same compound with a chlorine atom at position 2' (**17-F**). A geometry scan protocol, similar to that previously reported,[47] was applied. In particular, geometry scans are a series of jobs run that vary only the value of one or more variables used to define an internal or Cartesian coordinate in the input structure. A rigid geometry scan (without constraints on the ligand geometry) was conducted on both compounds. In this case the DFT/B3LYP 6-31G** level of theory was used in the gas phase, and the C19−N12−C11−C9 dihedral angle (herein defined as α) was varied in 13 steps from 0 to 360°.

ARs homology modelling. The A_{2A} structure, reported in Figure 4a, was chosen and used as template to generate the 3D structure of the other ARs (A_1, A_{2B}, and A_3). The A_{2A} and ARs sequences (of six different species, see Supplementary Figure S3) were aligned using the ClustalW server[48] (Supplementary Figure S3). Twenty 3D models for each AR were generated using Modeller 9.11[48] software. The obtained models were scored using the available scoring functions in Modeller9.11 software (DOPE score),[49] and through visual inspections. The protonation state of ionizable residues was fixed by using the Protein Preparation Wizard of the Maestro 9.1 graphical user interface, and then checked by visual inspection.[39]

The geometry of the final model was optimized using several cycles of OPLS2005 force field (available in Maestro) minimization, until a gradient of 0.001 kcal/mol*Å^2 was reached.

The loop of the optimized 3D models of the ARs were preliminary refined using the refinement loop tool available in Modeller 9.11 software, and also in this case the obtained loop models were scored using the available scoring functions in Modeller9.11 software, and through visual inspections. Finally, the obtained AR 3D structures were submitted to a loop refinement process using Prime,[39] and the refined protein structures were minimized using OPLSA2005 as force field, the PRCG methods until a gradient of 0.001 kcal/mol*Å^2 applying a stepwise relaxation protocol for which harmonic constraints were progressively reduced for backbone and side chains.

4.3. Biology

Materials. [^{3}H] CCPA ([^{3}H]2-chloro-*N*^{6}-cyclopentyladenosine; specific activity, 55 Ci/mmol), [^{3}H] CGS 21680 ([^{3}H] (2-[p-(2-carboxyethyl)-phenethylamino]-5'-N-ethylcarboxamido adenosine); specific activity, 41 Ci/mmol) and [^{125}I]AB-MECA ([^{125}I](4-aminobenzyl-5'-N-methylcarboxamido-adenosine); specific activity, 2200 Ci/mmol) were obtained from Perkin Elmer Research Products (Boston, MA). CCPA (2-chloro-N6-cyclopentyladenosine), CGS 21680 (2-[p-(2-carboxyethyl)-phenethylamino]-5'-*N*-ethyl-carboxamidoadenosine), NECA (*N*-ethyl-carboxamidoadenosine) and AB-MECA (4-aminobenzyl-5'-*N*-methylcarboxamidoadenosine) were obtained from Sigma (St. Louis, MO, USA). All other reagents were of analytical grade and obtained from commercial sources.

Cell membrane preparation. The hA_1CHO, hA_{2A}CHO and hA_3CHO cells were grown adherently and maintained in Dulbecco's modified Eagle's medium with nutrient mixture F12, containing 10% fetal calf serum, penicillin (100 U/mL), streptomycin (100 µg/mL), L-glutamine (2 mM), geneticine (G418) 0.2 mg/mL at 37 °C in 5% CO2/95% air. For membrane preparation the culture medium

was removed and the cells were washed with phosphate-buffered saline and scraped off T75 flasks in ice-cold hypotonic buffer (5 mM Tris HCl, 1 mM EDTA, pH 7.4). The cell suspension was homogenized with a Polytron, the homogenate was spun for 10 min at 1000 x g and the supernatant was then centrifuged for 30 min at 100,000 x g. The membrane pellet was suspended in 50 mM Tris HCl buffer (pH 7.4) for A_1ARs, in 50 mM Tris HCl, 10 mM $MgCl_2$ (pH 7.4) for A_{2A}ARs, in 50 mM Tris HCl, 10 mM $MgCl_2$, 1 mM EDTA (pH 7.4) for A_3ARs. The membranes were incubated with 2 IU/mL of adenosine deaminase to reduce the endogenous adenosine.[50]

Human cloned A_1, A_{2A} and A_3AR binding assay. All synthesized compounds were tested to evaluate their affinity to hA_1, hA_{2A} and hA_3ARs expressed in CHO membrane preparations as above described. Displacement experiments of [^{3}H]CCPA (1 nM) to hA_1 CHO membranes (50 μg of protein/assay) and at least six to eight different concentrations of novel compounds for 120 min at 25°C in 50 mM Tris HCl buffer pH 7.4 were performed.[51] Non-specific binding was determined in the presence of 1 μM of CCPA (≤ 10% of the total binding). Binding of [^{3}H]CGS 21680 (1 nM) to hA_{2A}CHO membranes (50 μg of protein/assay) was performed using 50 mM Tris HCl buffer, 10 mM $MgCl_2$ pH 7.4 and at least six to eight different concentrations of the ligands studied for an incubation time of 120 min at 25°C.[52] Non-specific binding was determined in the presence of 1 μM CGS 21680 and was about 20% of total binding. Competition binding experiments to hA_3 CHO membranes (50 μg of protein/assay) and 0.5 nM [^{125}I]AB-MECA, 50 mM Tris HCl buffer, 10 mM $MgCl_2$, 1 mM EDTA, pH 7.4 and at least six to eight different concentrations of examined ligands for 30 min at 37 °C.[53] Non-specific binding was defined as binding in the presence of 1 μM AB-MECA and was about 20% of total binding. Bound and free radioactivity were separated by filtering the assay mixture through Whatman GF/B glass fiber filters using a Brandel cell harvester. The filter bound radioactivity was counted by Scintillation Counter Packard Tri Carb 2810 TR with an efficiency of 62%.

Measurement of cyclic AMP levels in CHO cells. The hA_{2A} or hA_{2B}CHO cells ($1x10^6$ cells /assay) were suspended in 0.5 ml of incubation mixture (mM): NaCl 15, KCl 0.27, NaH_2PO_4 0.037, $MgSO_4$ 0.1, $CaCl_2$ 0.1, Hepes 0.01, $MgCl_2$ 1, glucose 0.5, pH 7.4 at 37 °C, 2 IU/ml adenosine deaminase and 4-(3-butoxy-4-methoxybenzyl)-2-imidazolidinone (Ro 20-1724) as phosphodiesterase inhibitor and preincubated for 10 min in a shaking bath at 37 °C. The potency expressed as EC_{50} (nM) of the novel compounds versus A_{2A}ARs or A_{2B}ARs was determined by the stimulation of cyclic AMP levels, respectively.[54] The reaction was terminated by the addition of cold 6% trichloroacetic acid (TCA). The TCA suspension was centrifuged at 2000 g for 10 min at 4 °C and the supernatant was extracted four times with water saturated diethyl ether. The final aqueous solution was tested for cyclic AMP levels by a competition protein binding assay. Samples of cyclic AMP standard (0-10 pmoles) were added to each test tube containing [^{3}H] cyclic AMP and the incubation buffer (trizma base 0.1 M, aminophylline 8.0 mM, 2-mercaptoethanol 6.0 mM, pH 7.4). The binding protein, previously prepared from beef adrenals, was added to the samples, incubated at 4 °C for 150 min, and after the addition of charcoal was centrifuged at 2000 g for 10 min. The clear supernatant was counted in a Scintillation Counter Packard Tri Carb 2810 TR.

Data Analysis. The protein concentration was determined according to a Bio-Rad method[55] with bovine albumin as a standard reference. Inhibitory binding constant (K_i) values were calculated from those of IC_{50} according to Cheng & Prusoff equation $K_i = IC_{50}/(1+[C^*]/K_D^*)$, where [C*] is the concentration of the radioligand and K_D^* its dissociation constant.[56] A weighted non linear least-squares curve fitting program LIGAND[57] was used for computer analysis of inhibition experiments. Functional experiments were analyzed by using the statistic software package GraphPad Prism 5.00. All experimental data are expressed as mean ± standard error of the mean (S.E.M.) of three or four independent experiments performed in duplicate.

ASSOCIATED CONTENT

Supporting Information Available: Synthetic procedures for the preparation of all reaction intermediates, final compounds and the amines **13a-ab**/**14a-k**, additional molecular modeling figures and MD protocol information, SMILES strings of final compounds **17**-**54**. This material is available free of charge via the Internet at http://pubs.acs.org.

AUTHOR INFORMATION

Corresponding authors

*For P.G.B.: phone, +39-0532-455921, Fax: +39-0532-455921, E-mail: baraldi@dns.unife.it.

*For S.C.: phone, +39-0823-274789, E-mail: sandro.cosconati@unina2.it.

ABBREVIATIONS USED

ARs, adenosine receptors; cAMP, 3',5'-cyclic adenosine monophosphate; CHO, chinese hamster ovary; PTP, pyrazolo[4,3-*e*][1,2,4]triazolo[1,5-*c*]pyrimidine; TCA, trichloroacetic acid; MD, molecular dynamics.

References

1. Fredholm, B. B. Adenosine receptors as drug targets. *Exp. Cell Res.* **2010**, *316*, 1284-1288.
2. Fredholm, B. B.; IJzerman, A. P.; Jacobson, K. A.; Linden, J.; Muller, C.E. International Union of Basic and Clinical Pharmacology. LXXXI. Nomenclature and classification of adenosine receptors-an update. *Pharmacol. Rev.* **2011**, *63*, 1-34.
3. de Lera Ruiz, M.; Lim, Y. H.; Zheng, J. Adenosine A_{2A} receptor as a drug discovery target. *J. Med. Chem.* **2013**, *57*, 3623-3650.

4. Muller, C. E.; Jacobson, K. A. Recent developments in adenosine receptor ligands and their potential as novel drugs. *Biochim. Biophys. Acta.* **2011**, *1808*, 1290-1308.

5. Yuan, G.; Jones, G. B. Towards next generation adenosine A_{2A} receptor antagonists. *Curr. Med. Chem.* **2014**, *21*, 3918-3935.

6. Rivera-Oliver, M.; Díaz-Ríos, M. Using caffeine and other adenosine receptor antagonists and agonists as therapeutic tools against neurodegenerative diseases: a review. *Life Sci.* **2014**, *101*, 1-9.

7. Lappas, C. M.; Sullivan, G. W.; Linden, J. Adenosine A_{2A} agonists in development for the treatment of inflammation. *Expert Opin. Investig. Drugs* **2005**, *14*, 797-806.

8. Varani, K.; Padovan, M.; Govoni, M.; Vincenzi. F.; Trotta, F.; Borea, P. A. The role of adenosine receptors in rheumatoid arthritis. *Autoimmun. Rev.* **2010**, *10*, 61–64.

9. Chen, J. F.; Eltzschig, H. K.; Fredholm, B. B. Adenosine receptors as drug targets-what are the challenges? *Nat. Rev. Drug Discov.* **2013**, *12*, 265-286.

10. Armentero, M. T.; Pinna, A.; Ferre, S.; Lanciego, J. L.; Muller, C. E.; Franco, R. Past, present and future of A_{2A} adenosine receptor antagonists in the therapy of Parkinson's disease. Pharmacol. Ther. **2011**, *132*, 280-299.

11. Varani, K.; Vincenzi, F.; Tosi, A.; Gessi, S.; Casetta, I.; Granieri, G.; Fazio, P.; Leung, E.; MacLennan, S.; Granieri, E.; Borea, P. A. A_{2A} adenosine receptor overexpression and functionality, as well as TNF-alpha levels, correlate with motor symptoms in Parkinson's disease. *FASEB J.* **2010**, *24*, 587-598.

12. Varani, K.; Bachoud-Lévi, A. C.; Mariotti, C.; Tarditi, A.; Abbracchio, M. P.; Gasperi, V.; Borea, P. A.; Dolbeau, G.; Gellera, C.; Solari, A.; Rosser, A.; Naji, J.; Handley, O.; Maccarrone, M.; Peschanski, M.; DiDonato, S.; Cattaneo, E. Biological abnormalities of peripheral A_{2A} receptors in a large representation of polyglutamine disorders and Huntington's disease stages. *Neurobiol. Dis.* **2007**, *27*, 36–43.

13. Pinna, A. Adenosine A_{2A} receptor antagonists in Parkinson's disease: progress in clinical trials from the newly approved Istradefylline to drugs in early development and those already discontinued. *CNS Drugs* **2014**, *28*, 455-474.

14. Headrick, J. P.; Ashton, K. J.; Rose'meyer, R. B.; Peart, J. N. Cardiovascular adenosine receptors: expression, actions and interactions. Pharmacol. Ther. **2013**, *140*, 92-111.

15. Gao, Z. G.; Jacobson, K. A. Emerging adenosine receptor agonists. *Expert Opin. Emerg. Drugs* **2007**, *12*, 479-492.

16. Varani, K.; Caramori, G.; Vincenzi, F.; Tosi, A.; Barczyk, A.; Contoli, M.; Casolari, P.; Triggiani, M.; Hansel, T.; Leung, E.; Maclennan, S.; Barnes, P. J.; Chung, K. F.; Adcock, I.; Papi, A.; Borea, P. A. Oxidative/nitrosative stress selectively altered A_{2B} adenosine receptors in chronic obstructive pulmonary disease. *FASEB J.* **2010**, 24, 1192-1204.

17. Varani, K.; Massara, A.; Vincenzi, F.; Tosi, A.; Padovan, M.; Trotta, F.; Borea, P. A. Normalization of A_{2A} and A_3 adenosine receptor up-regulation in rheumatoid arthritis patients by treatment with anti-tumor necrosis factor alpha but not methotrexate. *Arthritis Rheum.* **2009**, *60*, 2880-2891.

18. Varani, K.; Vincenzi, F.; Tosi, A.; Targa, M.; Masieri, F. F.; Ongaro, A.; De Mattei, M.; Massari, L.; Borea, P. A. Expression and functional role of adenosine receptors in regulating inflammatory responses in human synoviocytes. *Br. J. Pharmacol.* **2010**, *160*, 101–115.

19. Varani, K.; Padovan, M.;, Vincenzi, F.; Targa, M.; Trotta, F.; Govoni, M.; Borea, P. A. A_{2A} and A_3 adenosine receptor expression in rheumatoid arthritis: upregulation, inverse correlation with disease activity score and suppression of inflammatory cytokine and metalloproteinase release. *Arthritis Res. Ther.* **2011**, *13*, R197.

20. Vincenzi, F.; Padovan, M.; Targa, M.; Corciulo, C.; Giacuzzo, S.; Merighi, S.; Gessi, S.; Govoni, M.; Borea, P. A.; Varani, K. A_{2A} adenosine receptors are differentially modulated

by pharmacological treatments in rheumatoid arthritis patients and their stimulation ameliorates adjuvant-induced arthritis in rats. *PLoS One* **2013**, *8*, e54195.

21. Mazzon, E.; Esposito, E.; Impellizzeri, D.; DI Paola, R.; Melani, A.; Bramanti, P.; Pedata, F.; Cuzzocrea, S. CGS 21680, an agonist of the adenosine A_{2A} receptor, reduces progression of murine type II collagen-induced arthritis. *J. Rheumatol.* **2011**, *38*, 2119-2129.
22. Beattie, D.; Brearley, A.; Brown, Z.; Charlton, S. J.; Cox, B.; Fairhurst, R. A.; Fozard, J. R.; Gedeck, P.; Kirkham, P.; Meja, K.; Nanson, L.; Neef, J.; Oakman, H.; Spooner, G.; Taylor, R. J.; Turner, R. J.; West, R.; Woodward, H. Synthesis and evaluation of two series of 4'-aza-carbocyclic nucleosides as adenosine A_{2A} receptor agonists. *Bioorg. Med. Chem. Lett.* **2010**, *20*, 1219-1224.
23. Deflorian, F.; Kumar, T. S.; Phan, K.; Gao, Z. G.; Xu, F.; Wu, H.; Katritch, V.; Stevens, R. C.; Jacobson, K. A. Evaluation of molecular modeling of agonist binding in light of the crystallographic structure of an agonist-bound A_{2A} Adenosine Receptor. *J. Med. Chem.* **2012**, *55*, 538-552.
24. Jaakola, V. P.; Griffith, M. T.; Hanson, M. A.; Cherezov, V.; Chien, E. Y.; Lane, J. R.; Ijzerman, A. P.; Stevens, R. C. The 2.6 angstrom crystal structure of a human A_{2A} adenosine receptor bound to an antagonist. *Science* **2008**, *322*, 1211-1217.
25. Lebon, G.; Warne, T.; Edwards, P. C.; Bennett, K.; Langmead, C. J.; Leslie, A. G.; Tate, C. G. Agonist-bound adenosine A_{2A} receptor structures reveal common features of GPCR activation. *Nature* **2011**, *474*, 521-525.
26. Kim, S. K.; Gao, Z. G.; Van Rompaey. P.; Gross, A. S.; Chen, A.; Van Calenbergh, S.; Jacobson, K. A. Modeling the adenosine receptors: comparison of the binding domains of A_{2A} agonists and antagonists. *J. Med. Chem.* **2003**, *46*, 4847-4859.

27. Vu, C. B.; Shields, P.; Peng, B.; Kumaravel, G.; Jin, X.; Phadke, D.; Wang, J.; Engber, T.; Ayyub, E.; Petter, R. C. Triamino derivatives of triazolotriazine and triazolopyrimidine as adenosine A_{2A} receptor antagonists. *Bioorg. Med. Chem. Lett.* **2004**, *14*, 4835-4838.

28. Hutchison, H. J.; Williams, M.; De Jesus, R.; Yokoyama, R.; Oei, H. H.; Ghai, G. R.; Webb, R. L.; Zoganas, H. C.; Stone, G. A.; Jarvis, M. F. 2-(Arylalkylamino)adenosin-5'-uronamides: a new class of highly selective adenosine A_2 receptor ligands. *J. Med. Chem.* **1990**, *33*, 1919-1924.

29. Jung, H. K.; Doddareddy, M. R.; Cha, J. H.; Rhim, H.; Cho, Y. S.; Koh, H. Y.; Jung, B. Y.; Pae, A. N. Synthesis and biological evaluation of novel T-type Ca^{2+} channel blockers. *Bioorg. Med. Chem.* **2004**, *12*, 3965-3970.

30. Giblin, G. M. P.; Healy, M. P. Isoindol derivatives as EP4 receptor agonists. WO2008046798.

31. Carceller, E.; Jimenez, P. J. Novel piperidines and piperazines as platelet aggregation inhibitors. WO9920606.

32. Kubota, D.; Ishikawa, M.; Yamamoto, M.; Murakami, S.; Hachisu, M.; Katano, K.; Ajito, K. Tricyclic pharmacophore-based molecules as novel integrin $\alpha_v\beta_3$ antagonists. Part 1: design and synthesis of a lead compound exhibiting $\alpha_v\beta_3/\alpha_{IIb}\beta_3$ dual antagonistic activity. *Bioorg. Med. Chem.* **2006**, *14*, 2089-2108.

33. Jung, H. K.; Doddareddy, M. R.; Cha, J. H.; Rhim, H.; Cho, Y.S.; Koh, H. Y.; Jung, B. Y.; Pae, A. N. Synthesis and in vitro evaluation of oxindole derivatives as potential radioligands for 5-HT7 receptor imaging with PET. *ACS Chem. Neurosci.* **2012**, *3*, 1002-1007.

34. Schmidtke, P.; Luque, F. J.; Murray, J. B.; Barril, X. Shielded hydrogen bonds as structural determinants of binding kinetics: application in drug design. *J. Am. Chem. Soc.* **2011**, *133*, 18903-18910.

35. Bruno, A.; Costantino, G. Molecular dynamics simulations of G Protein-Coupled Receptors. *Mol. Inform.* **2012**, *31*, 222-230.

36. Colizzi, F.; Perozzo, R.; Scapozza, L.; Recanatini, M.; Cavalli, A. Single-molecule pulling simulations can discern active from inactive enzyme inhibitors. *J. Am. Chem. Soc.* **2010**, *132*, 7361-7371.

37. Capelli, A. M.; Bruno, A.; Entrena Guadix, A.; Costantino, G. Unbinding pathways from the glucocorticoid receptor shed light on the reduced sensitivity of glucocorticoid ligands to a naturally occurring, clinically relevant mutant receptor. *J. Med. Chem.* **2013**, *56*, 7003-7014.

38. Xu. F.; Wu, H.; Katritch, V.; Han, G. W.; Jacobson, K. A.; Gao, Z. G.; Cherezov, V.; Stevens, R. C. Structure of an agonist-bound human A_{2A} adenosine receptor. *Science* **2011**, *332*, 322-327.

39. Schrödinger, Mestro version 9.1 Schrödinger, LLC, New York 2009 http://www.schrodinger.com/

40. Bruno, A.; Beato, C.; Costantino, G. Molecular dynamics simulations and docking studies on 3D models of the heterodimeric and homodimeric 5-HT_{2A} receptor subtype. *Future Med. Chem.* **2011**, *3*, 665–681.

41. Bruno, A.; Entrena Guadix, A..; Costantino, G. Molecular dynamics simulation of the heterodimeric mGluR2/$5HT_{2A}$ complex. An atomistic resolution study of a potential new target in psychiatric conditions. *J. Chem. Inf. Model.* **2009**, *49*, 1602-1616.

42. Bruno, A.; Costantino, G.; de Fabritiis, G.; Pastor, M.; Selent, J. Membrane-sensitive conformational states of helix 8 in the metabotropic Glu2 receptor, a class C GPCR. *PLoS ONE*, **2012**, *7*, e42023.

43. Phillips, J. C.; Braun, R.; Wang, W.; Gumbart, J.; Tajkhorshid, E.; Villa, E.; Chipot, C.; Skeel, R. D.; Kalé, L.; Schulten, K. Scalable molecular dynamics with NAMD. *J. Comput. Chem.* **2005**, *26*, 1781-1802.

44. NAMD - Scalable Molecular Dynamics http://www.ks.uiuc.edu/Research/namd/)

45. The Amber Molecular Dynamics Package ambermd.org http://ambermd.org/)

46. http://www.gaussian.com/g_misc/g03/g03_rel.htm#e1

47. Castellano, S.; Taliani, S.; Viviano, M.; Milite, C.; Da Pozzo, E.; Costa, B.; Barresi, E.; Bruno, A.; Cosconati, S.; Marinelli, L.; Greco, G.; Novellino, E.; Sbardella, G.; Da Settimo, F.; Martini, C. Structure-activity relationship refinement and further assessment of 4-phenylquinazoline-2-carboxamide translocator protein ligands as antiproliferative agents in human glioblastoma tumors. *J. Med. Chem.* **2014**, *57*, 2413–2428

48. ClustalW2 - Multiple Sequence Alignment http://www.ebi.ac.uk/Tools/msa/clustalw2/

49. MODELLER, Program for Comparative Protein Structure Modelling by Satisfaction of Spatial Restraints http://salilab.org/modeller

50. Varani, K.; Merighi, S.; Gessi, S.; Klotz, K. N.; Leung, E.; Baraldi, P. G.; Cacciari, B.; Romagnoli, R.; Spalluto, G.; Borea, P.A. [^{3}H]MRE 3008F20: a novel antagonist radioligand for the pharmacological and biochemical characterization of human A_3 adenosine receptors. *Mol. Pharmacol.* **2000**, *57*, 968-975.

51. Romagnoli, R.; Baraldi, P. G.; Carrion, M. D.; Cara, C. L.; Cruz-Lopez, O.; Salvador, M. K.; Preti, D.; Aghazadeh Tabrizi, M.; Moorman, A. R.; Vincenzi, F.; Borea, P. A.; Varani, K. Synthesis and biological evaluation of 2-amino-3-(4-chlorobenzoyl)-4-[(4-arylpiperazin-1-yl)methyl]-5-substituted-thiophenes. Effect of the 5-modification on allosteric enhancer activity at the A_1 adenosine receptor. *J. Med. Chem.* **2012**, *55*, 7719-7735.

52. Varani, K.; Gessi, S.; Dalpiaz, A.; Borea, P. A. Pharmacological and biochemical characterization of purified A_{2A} adenosine receptors in human platelet membranes by [^{3}H]-CGS 21680 binding. *Br. J. Pharmacol.* **1996**, *117*, 1693-1701.

53. Varani, K.; Cacciari, B.; Baraldi, P.G.; Dionisotti, S.; Ongini, E.; Borea, P. A. Binding affinity of adenosine receptor agonists and antagonists at human cloned A_3 adenosine receptors. *Life Sci.***1998**, *63*, 81-87.

54. Varani, K.; Gessi, S.; Merighi, S.; Vincenzi, F.; Cattabriga, E.; Benini, A.; Klotz, K. N.; Baraldi, P. G.; Aghazadeh Tabrizi, M.; Lennan, S. M.; Leung, E.; Borea, P. A. Pharmacological characterization of novel adenosine ligands in recombinant and native human A_{2B} receptors. *Biochem. Pharmacol.* **2005**, *70*, 1601-1612.

55. Bradford, M. M. A rapid and sensitive method for the quantification of microgram quantities of protein utilizing the principle of protein dye-binding. *Anal. Biochem.* **1976**, *72*, 248-254.

56. Cheng, Y.; Prusoff, W. H. Relationships between the inhibition constant (K_i) and the concentration of inhibitor which causes 50 per cent inhibition (IC_{50}) of an enzymatic reaction. *Biochem. Pharmacol.* **1973**, *22*, 3099-3108.

57. Munson, P. J.; Rodbard, D. Ligand: a versatile computerized approach for the characterization of ligand binding systems. *Anal. Biochem.* **1980**, *107*, 220-239.

Figure Legends

Figure 1. Overview of some of the most representative A_{2A}AR agonists reported so far.

Figure 2. (a) Superposition of the **ZM241385** (cyan spheres and sticks), **NECA** (green spheres and sticks), and **UKA432097** (orange spheres and sticks) bound to the A_{2A}AR (white cartoon). Highlighted by red arrows the C^5-position (**ZM241385**) and the C^2-position (**NECA** and **UKA432097**), which overlaps in the reported binding modes. Structures were obtained from the 3EML,[14] 2YDV[15] and 3QAK.[23] X-ray crystal structures. Experimental X-ray complex between the A_{2A}AR and ZM241385 (**b**) and UKA432097 (**c**), interacting residues are also displayed.

Figure 3. Design of new A_{2A}AR agonists from known antagonists.

Figure 4. (a) Binding mode of **17** into the A_{2A}AR binding pocket. Receptor residues and **17** are depicted in white and orange sticks, respectively. In the insets the A_{2B}AR, A_1AR, and A_3AR (pink, purple and green sticks, respectively) are depicted by outlining the critical differences that with the A_{2A}AR that are supposed to be responsible for the selectivity of **17** for the latter AR subtype. The A_{2A}AR structure is depicted in white-transparent cartoon, while the ECL2 of the same receptor in cyan-transparent cartoon. (**b**) rmsd of the **17** heavy atoms, along 100ns long MD simulation with respect to the binding mode reported in (**a**). (**c**) Superposition of the binding mode obtained for **J42** and **17**.

Figure 5. (a) α dihedral angle distribution along the 100 ns long MD simulations for **17**, highlighted in the inset. (**b)** QM energy scan for **17** (black line and bars) and **17-F** (red line and bars) along the α dihedral angle. In the inset a comparison of the piperazinyl-phenyl conformer of **17** (orange sticks) observed in the proposed binding mode (Figure 3a), and the energetic minimum for the same group of **17-Cl** (yellow sticks and chlorine atom in green) obtained in the QM energy scan is reported.

Figure 6. Competition curves of specific [^{3}H]-CGS 21680 binding (A) and stimulatory curves of cAMP accumulation (B) to hA_{2A}ARs expressed in CHO cells by selected novel A_{2A}AR agonists. Values are the means and vertical lines are the SEM of three or four separate experiments as described in Experimental Section.

Figure 1

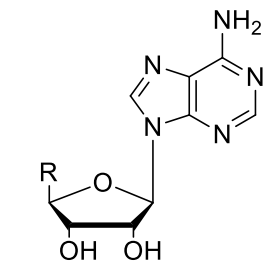

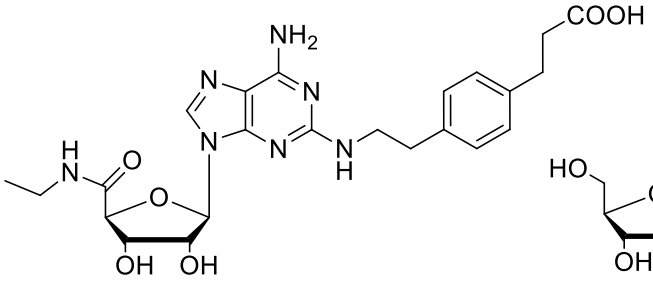

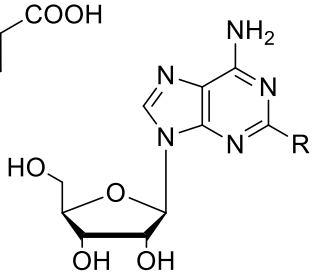

1a, Adenosine: R = CH_2OH
1b, NECA: R = CONHEt

2, CGS21680

3, Sonedenoson: R =

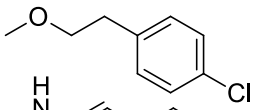

4, Binodenoson: R =

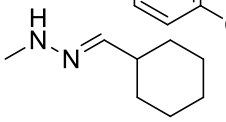

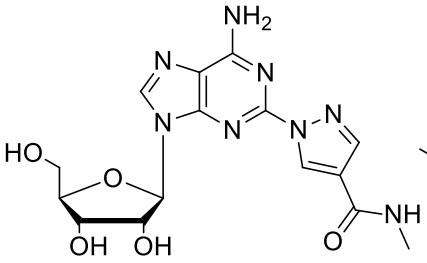

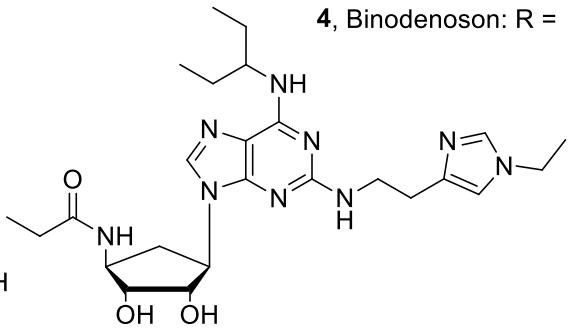

5, Regadenoson (CV-3146)

6

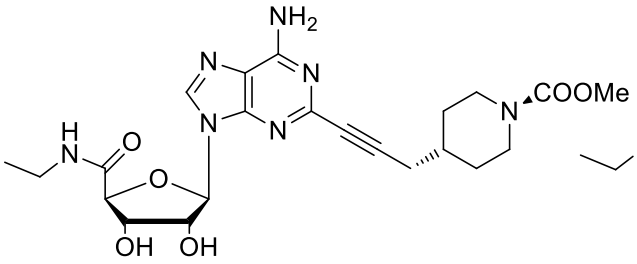

7, Apadenoson

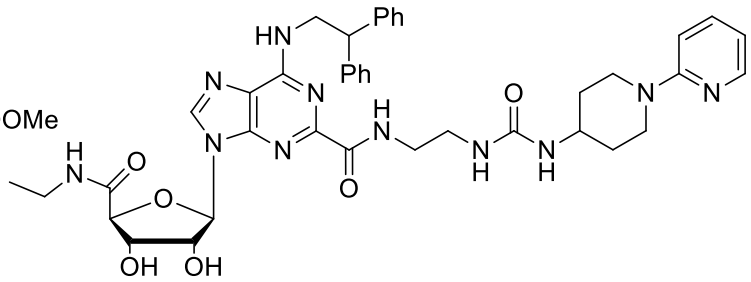

8, UK-432097

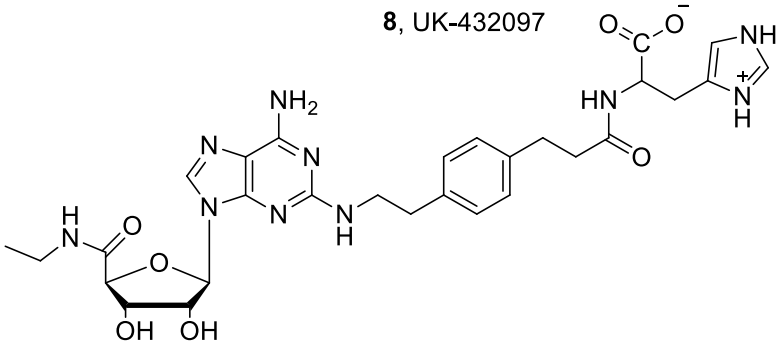

9, J42

Figure 2

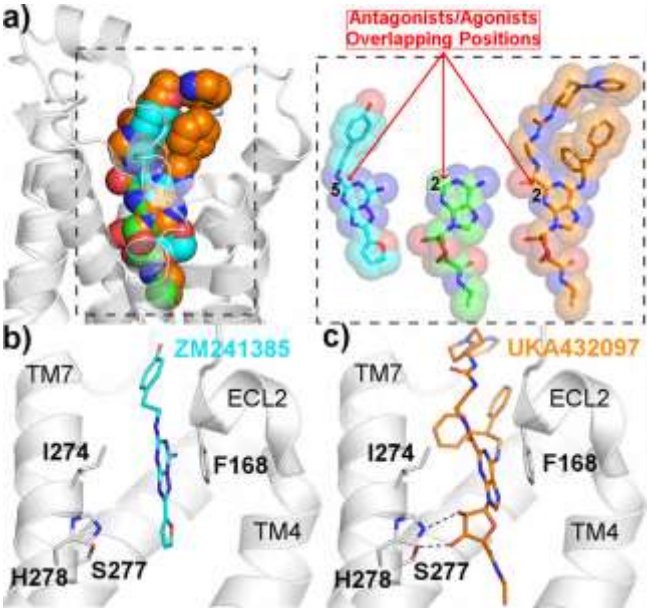
a)
Antagonists/Agonists
Overlapping Positions
5
2
2
b)
ZM241385
TM7
ECL2
I274
F168
TM4
H278
S277
c)
UKA432097
TM7
ECL2
I274
F168
TM4
H278
S277

Figure 3

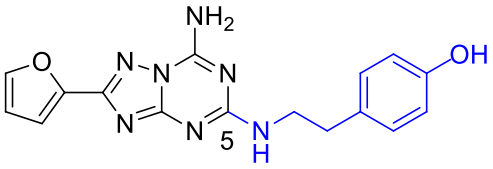

10, ZM241385

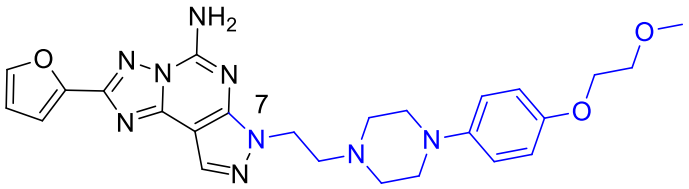

11, Preladenant, SCH420814

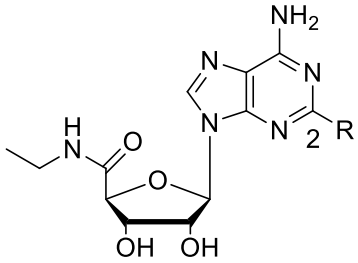

17-43, R = 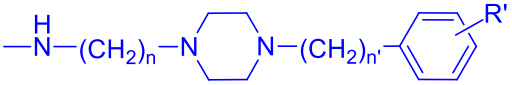

44-54, R = 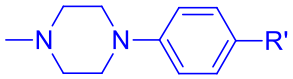

Figure 4

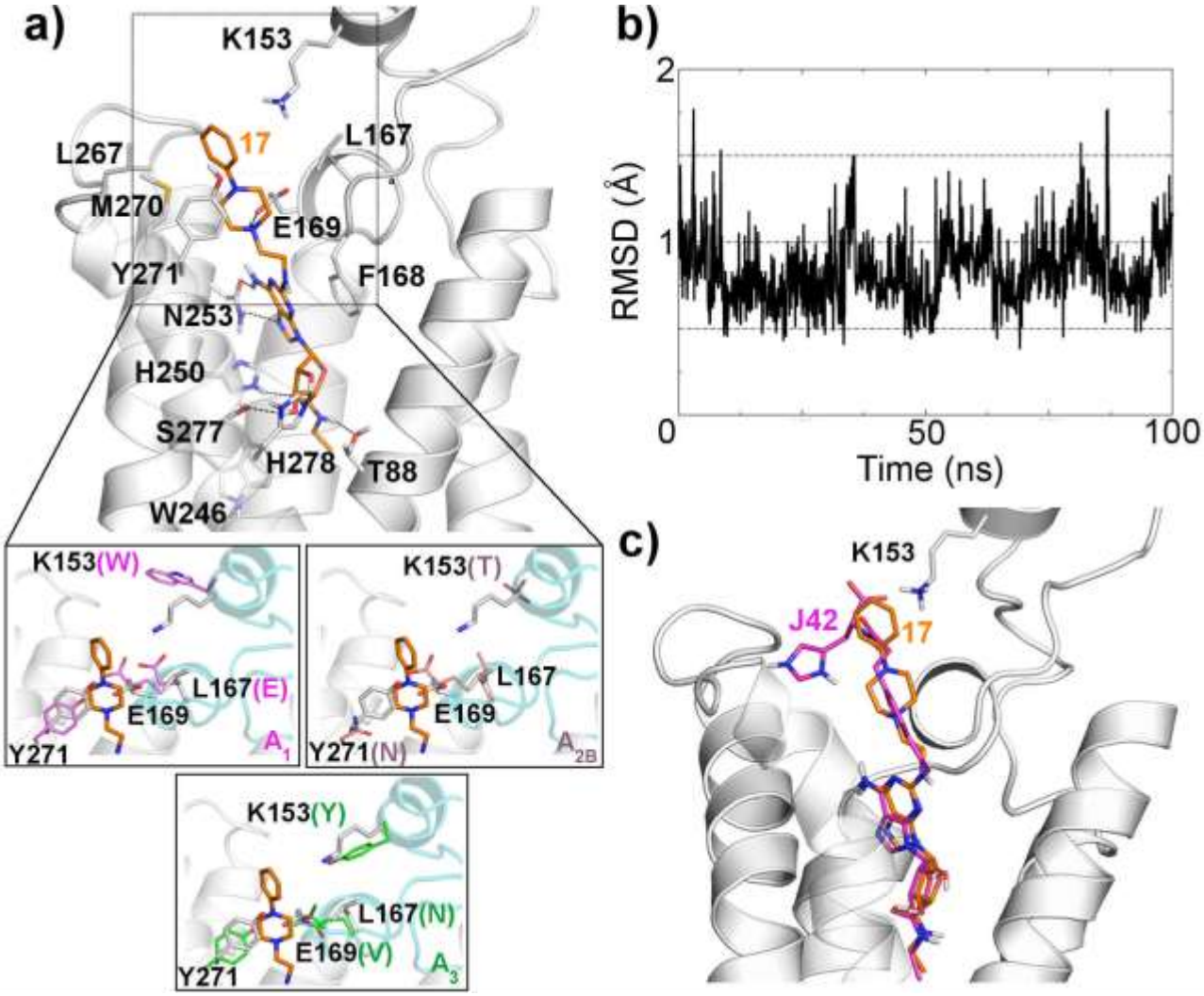
a)
K153
17
L267
L167
M270
E169
Y271
F168
N253
H250
S277
H278
T88
W246
K153(W)
L167(E)
E169
Y271
A1
K153(T)
L167
E169
Y271(N)
A2B
K153(Y)
L167(N)
E169(V)
Y271
A3
b)
RMSD (Å)
2
1
0
50
100
Time (ns)
c)
K153
J42
17

Figure 5

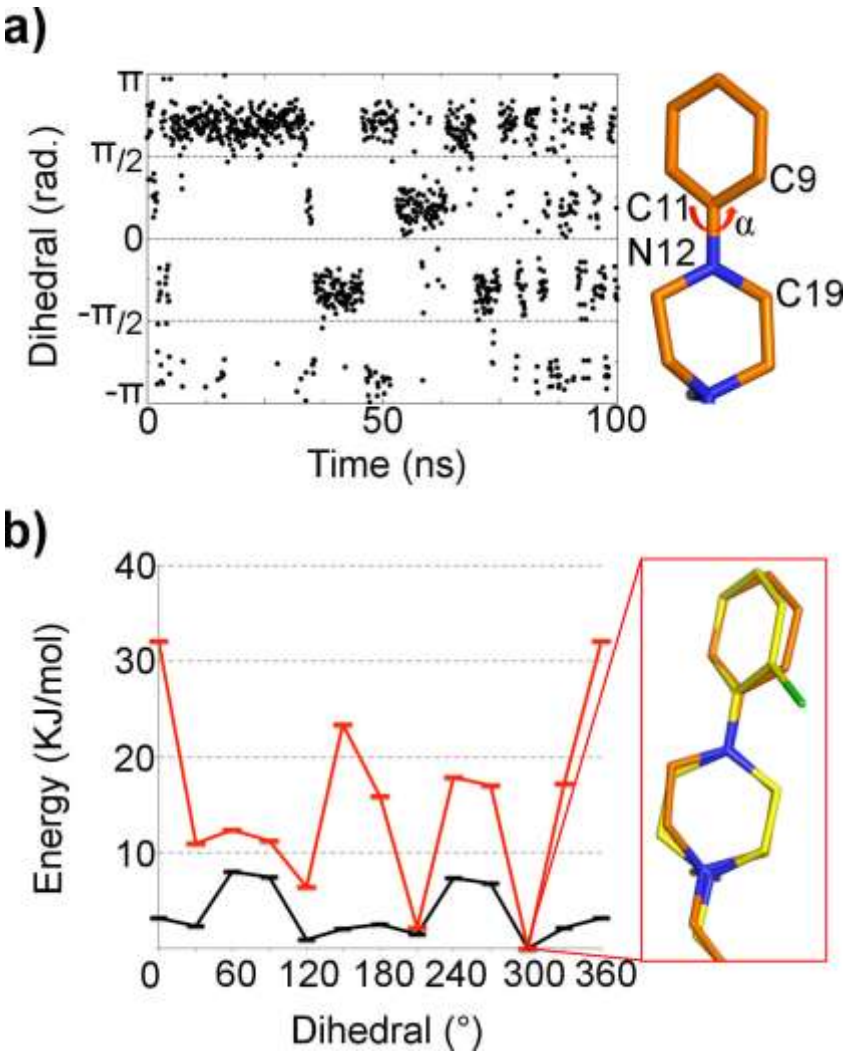
a)
π
π/2
0
-π/2
-π
Dihedral (rad.)
0
50
100
Time (ns)
C9
C11
α
N12
C19
b)
40
30
20
10
Energy (KJ/mol)
0
60
120
180
240
300
360
Dihedral (°)

Figure 6

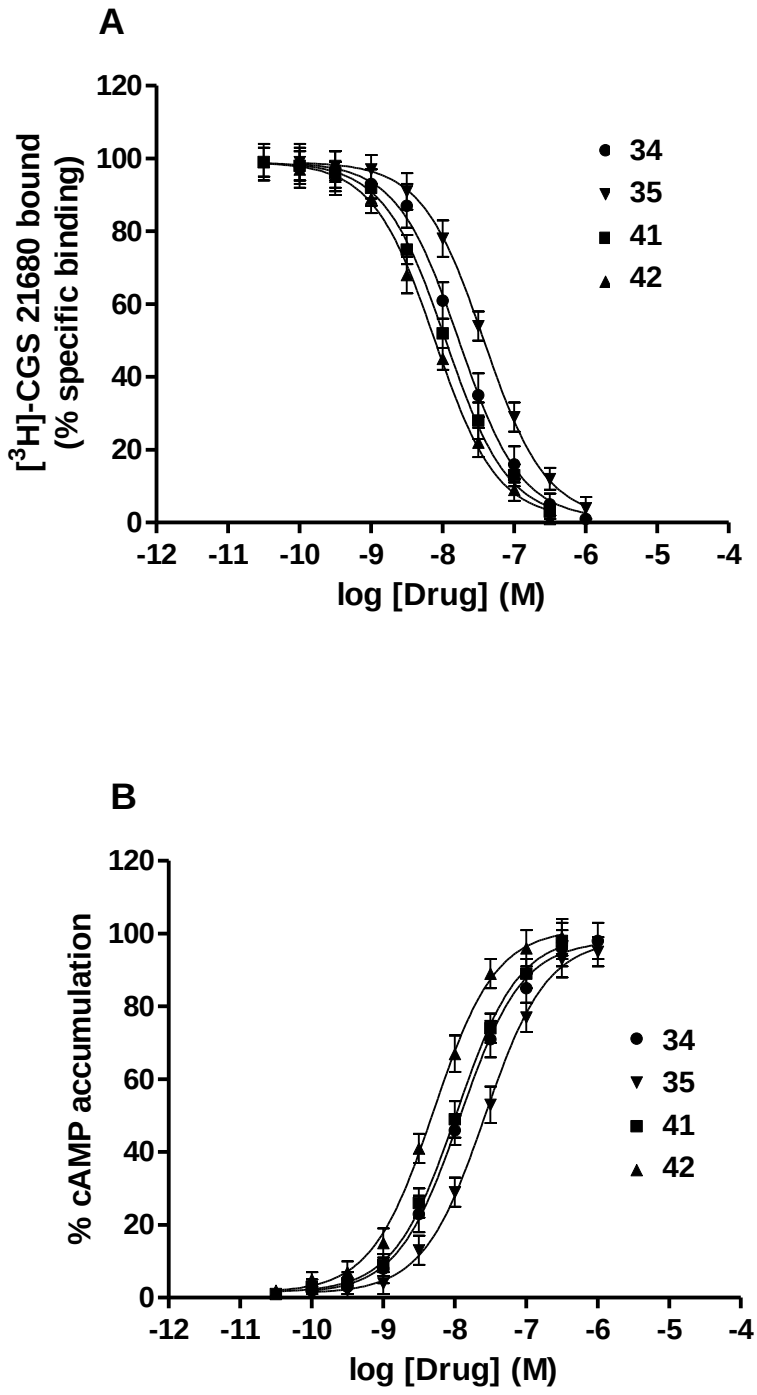
A
[3H]-CGS 21680 bound
(% specific binding)
120
100
80
60
40
20
0
-12
-11
-10
-9
-8
-7
-6
-5
-4
log [Drug] (M)
34
35
41
42
B
% cAMP accumulation
120
100
80
60
40
20
0
-12
-11
-10
-9
-8
-7
-6
-5
-4
log [Drug] (M)
34
35
41
42

Scheme 1[a]

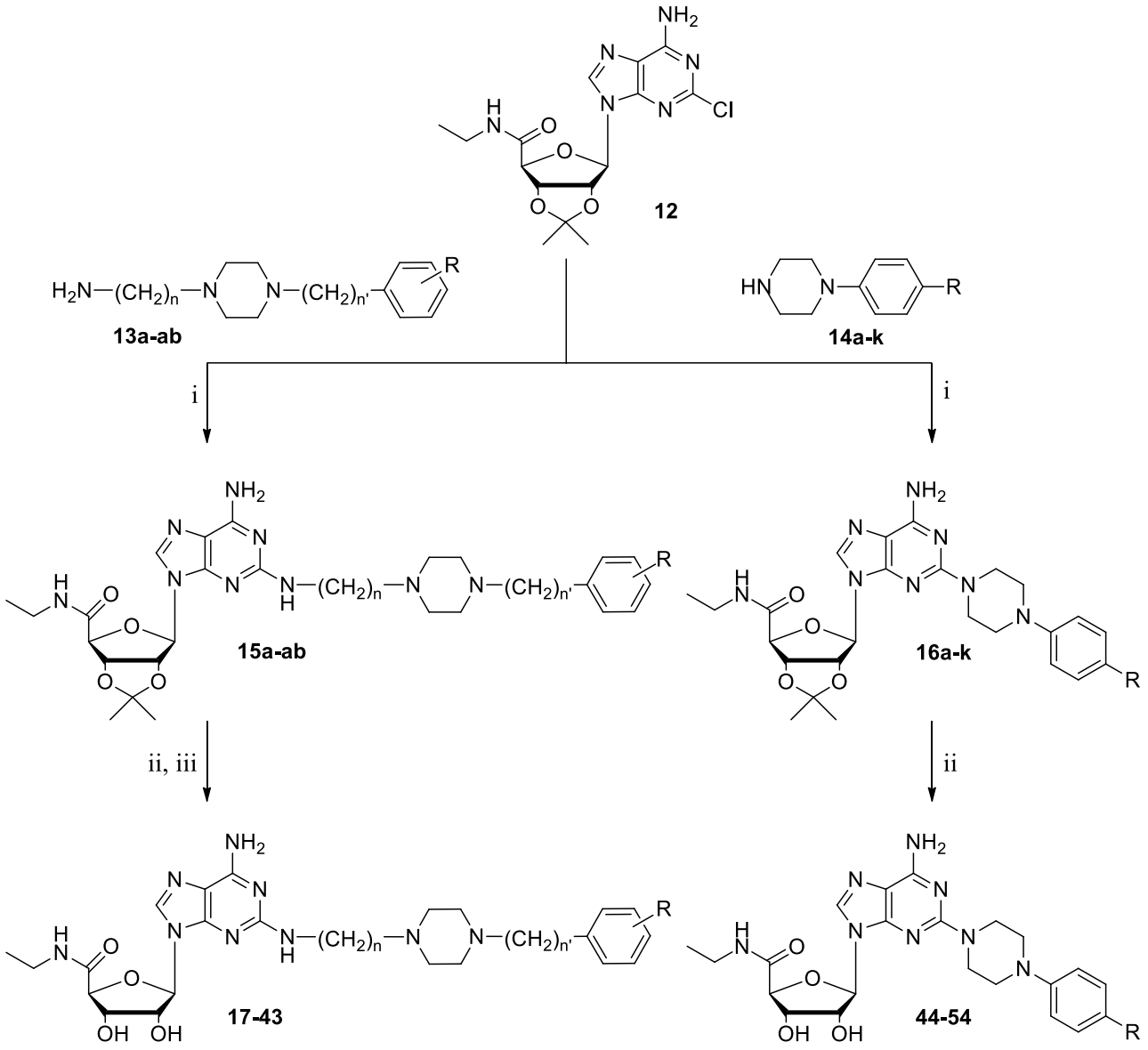

[a]Reagents and Conditions: i) TEA, DMSO, 120 °C, 24 h; ii) TFA/H_2O, rt, 4h; iii) only for compounds **30**, **31**, **33** and **43**, NaOH aq.(5%), MeOH, rt, 1h.

Scheme 2a[a]

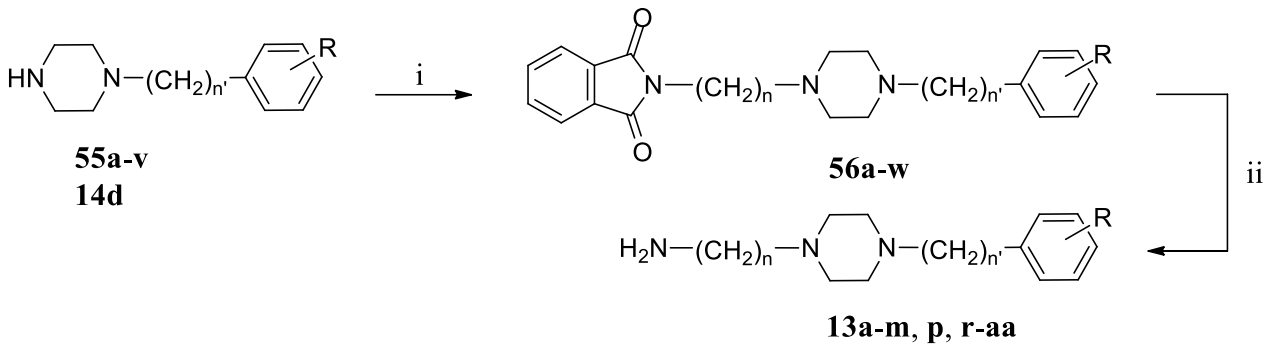

Scheme 2b[a]

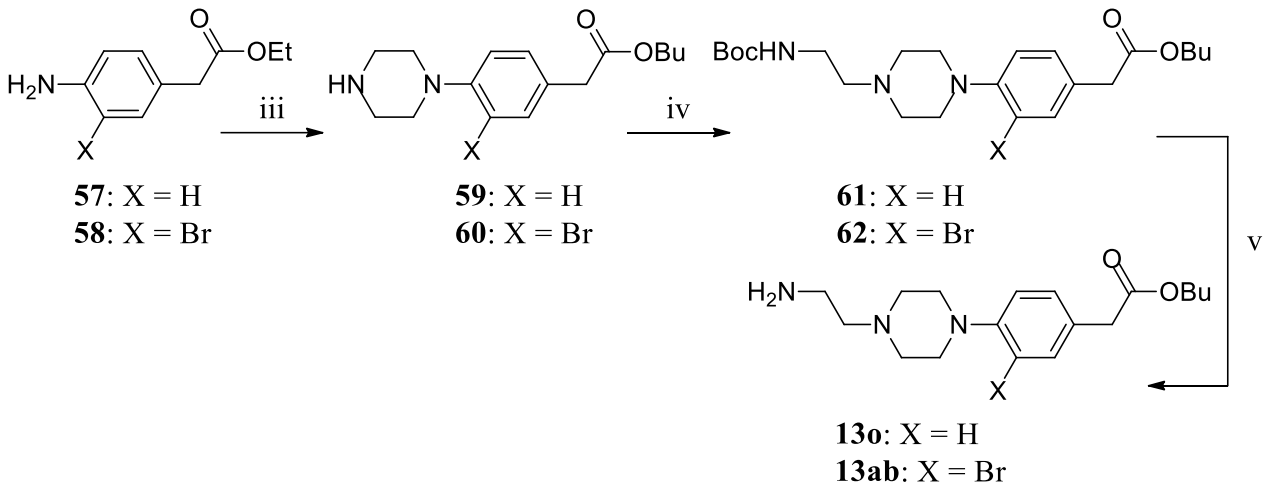

[a]Reagents and conditions: i) *N*-(2-bromoethyl)phthalimide or *N*-(3-bromopropyl)phthalimide, K_2CO_3, DMF, 80 °C, 4/6 h; ii) NH_2NH_2, EtOH, reflux, 4 h; iii) a. Bis(2-chloroethyl)amine, *n*-ButOH, reflux, 24 h; b. K_2CO_3, reflux, 24 h; iv) *N*-Boc-2-bromoethyl-amine, K_2CO_3, DMF, 80 °C, 18 h; v) TFA, CH_2Cl_2, rt, 1 h.

Scheme 3a[a]

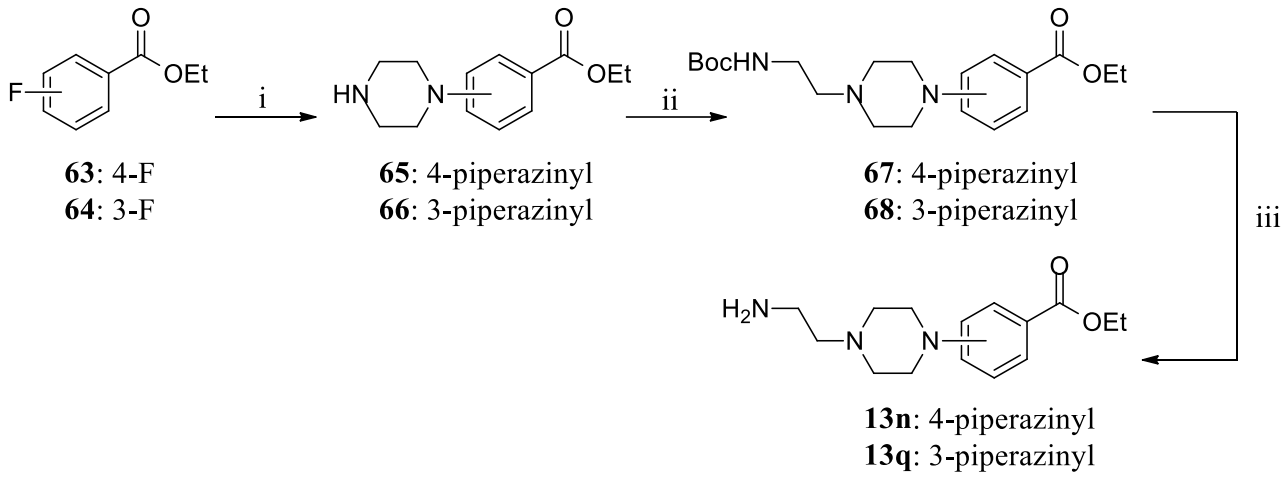

Scheme 3b[a]

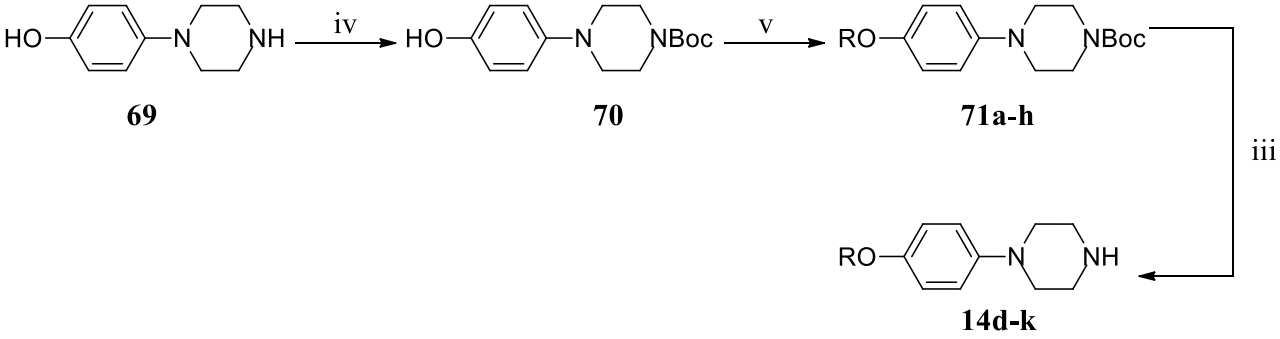

[a]Reagents and conditions: i) Piperazine, DMSO, 120 °C, 18 h; ii) *N*-Boc-2-bromoethyl-amine, K_2CO_3, DMF, 80 °C, 18 h; iii) TFA, CH_2Cl_2, rt, 1 h; iv) Di-*tert*-butyl dicarbonate, $NaHCO_3$, THF/H_2O/1,4-dioxane, rt, 18 h; v) Alkyl halides, NaH, CH_3CN, 50 °C, 4h.

Table 1. Affinity, potency and selectivity of compounds **17**-**20** and **44** to AR subtypes.

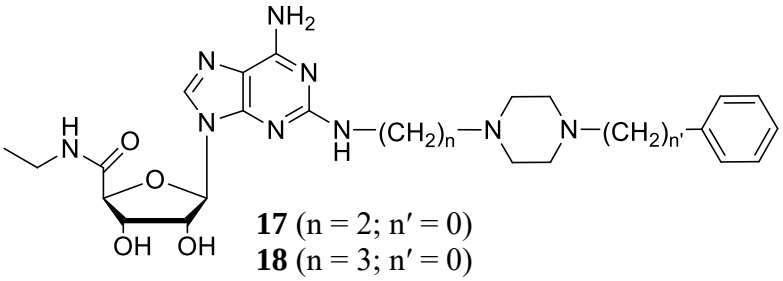

17 (n = 2; n′ = 0)
18 (n = 3; n′ = 0)
19 (n = 2; n′ = 1)
20 (n = 2; n′ = 2)

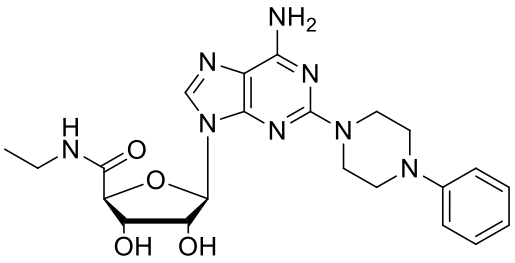

44

	hA$_1$ARs	**hA$_{2A}$ARs**	**hA$_{2A}$ARs**	**hA$_{2B}$ARs**	**hA$_3$ARs**
	***K*$_i$ (nM)**[a]	***K*$_i$ (nM)**[b]	**EC$_{50}$ (nM)**[c]	**EC$_{50}$ (nM)**[d]	***K*$_i$ (nM)**[e]
17	> 10000 (15%)	55 ± 5	91 ± 8	> 10000 (26%)	2161 ± 208
18	> 10000 (13%)	237 ± 22	438 ± 39	> 10000 (15%)	5502 ± 421
19	> 10000 (10%)	659 ± 67	842 ± 75	> 10000 (4%)	3252 ± 313
20	> 10000 (5%)	967 ± 84	1763 ± 162	> 10000 (5%)	4083 ± 396
44	> 10000 (10%)	> 10000 (32%)	> 10000 (18%)	> 10000 (10%)	> 10000 (12%)

[a]Displacement of specific [^{3}H]CCPA binding in membranes from hA$_1$CHO cells. [b]Displacement of specific [^{3}H]CGS21680 binding in membranes from hA$_{2A}$CHO cells. [c]Potency (EC$_{50}$) of examined compounds to stimulate cAMP levels in hA$_{2A}$CHO cells. [d]Potency (EC$_{50}$) of examined compounds to stimulate cAMP levels in hA$_{2B}$ CHO cells. [e]Displacement of specific [^{125}I]AB-MECA binding in membranes from hA$_3$CHO cells. The values are expressed as the mean ± SEM, n=3-6 independent experiments. In parentheses are reported the % of inhibition to hA$_1$, A$_{2A}$, A$_{2B}$ and A$_3$ CHO cells.

Table 2. Affinity, potency and selectivity of compounds **17**, and **21-43** to AR subtypes.

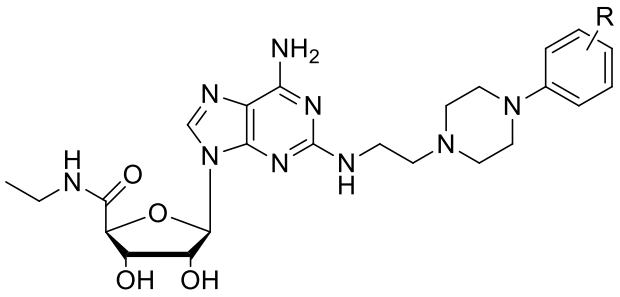

	R	**hA$_1$ARs**	**hA$_{2A}$ARs**	**hA$_{2A}$ARs**	**hA$_{2B}$ARs**	**hA$_3$ARs**
		***K*$_i$ (nM)**[a]	***K*$_i$ (nM)**[b]	**EC$_{50}$ (nM)**[c]	**EC$_{50}$ (nM)**[d]	***K*$_i$ (nM)**[e]
NECA	-	8.62 ± 0.78	8.41 ± 0.77	12.58 ± 1.12	262 ± 30	30 ± 4
CGS21680	-	> 10000 (17%)	12.48 ± 1.21	18.47 ± 1.88	> 10000 (23%)	384 ± 32
17	H	> 10000 (15%)	55 ± 5	91 ± 8	> 10000 (26%)	2161 ± 208
21	4-F	> 10000 (12%)	98 ± 8	145 ± 13	> 10000 (18%)	1874 ± 175
22	4-Cl	> 10000 (9%)	25 ± 3	31 ± 3	9287 ± 786	1677 ± 155
23	4-Br	> 10000 (17%)	29 ± 3	43 ± 5	9352 ± 824	1306 ± 127
24	4-I	> 10000 (11%)	92 ± 9	156 ± 14	7130 ± 645	3382 ± 314
25	4-CF_3	> 10000 (6%)	36 ± 4	47 ± 5	> 10000 (44%)	2034 ± 187
26	4-NO_2	> 10000 (13%)	24 ± 2	36 ± 4	> 10000 (30%)	759 ± 68

27	4-CH_3	> 10000 (12%)	88 ± 9	112 ± 10	> 10000 (37%)	2655 ± 218
28	4-OCH_3	> 10000 (17%)	43 ± 4	62 ± 6	> 10000 (25%)	2052 ± 194
29	4-$OCH_2CH_2OCH_3$	> 10000 (14%)	56 ± 6	84 ± 7	> 10000 (29%)	2195 ± 206
30	4-COOH	> 10000 (1%)	30 ± 2	38 ± 4	> 10000 (14%)	5833 ± 514
31	4-CH_2COOH	> 10000 (10%)	84 ± 8	103 ± 9	> 10000 (38%)	5884 ± 472
32	3-Cl	> 10000 (14%)	23 ± 2	46 ± 5	> 10000 (22%)	1172 ± 103
33	3-COOH	> 10000 (1%)	72 ± 6	95 ± 8	> 10000 (10%)	>10000 (29%)
34	2-F	> 10000 (7%)	7.76 ± 0.58	11.87 ± 1.17	> 10000 (37%)	1870 ± 173
35	2-Cl	> 10000 (7%)	18.21 ± 1.95	24 ± 2	> 10000 (32%)	1387 ± 118
36	2-CF_3	> 10000 (1%)	95 ± 8	127 ± 11	> 10000 (14%)	3425 ± 314
37	2-OMe	> 10000 (1%)	277 ± 25	393 ± 36	> 10000 (3%)	1845 ± 171
38	3-Cl, 4-F	> 10000 (16%)	34 ± 3	41 ± 3	> 10000 (25%)	1538 ± 136

39	3-Cl, 4-Cl	> 10000 (18%)	26± 2	38 ± 4	> 10000 (29%)	764 ± 71
40	3-Cl, 5-Cl	> 10000 (2%)	33 ± 2	53 ± 5	> 10000 (15%)	1003 ± 98
41	2-F, 3-F	> 10000 (8%)	5.48 ± 0.39	10.16 ± 1.09	> 10000 (19%)	1818 ± 175
42	2-F, 4-Cl	> 10000 (3%)	4.78 ± 0.41	4.89 ± 0.38	> 10000 (27%)	1487 ± 142
43	2-Br, 4-CH_2COOH	> 10000 (1%)	24 ± 2	48 ± 5	> 10000 (29%)	3481 ± 316

[a]Displacement of specific [^{3}H]CCPA binding in membranes from hA_1CHO cells. [b]Displacement of specific [^{3}H]CGS21680 binding in membranes from hA_{2A}CHO cells. [c]Potency (EC_{50}) of examined compounds to stimulate cAMP levels in hA_{2A}CHO cells. [d]Potency (EC_{50}) of examined compounds to stimulate cAMP levels in hA_{2B} CHO cells. [e]Displacement of specific [^{125}I]AB-MECA binding in membranes from hA_3CHO cells. The values are expressed as the mean ± SEM, n=3-6 independent experiments. In parentheses are reported the % of inhibition to hA_1, A_{2A} , A_{2B} and A_3 CHO cells.

Table 3. Affinity, potency and selectivity of compounds **44-54** to AR subtypes.

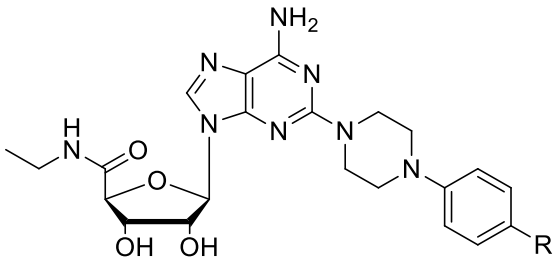

	R	**hA$_1$ARs** ***K*$_i$ (nM)**[a]	**hA$_{2A}$ARs** ***K*$_i$ (nM)**[b]	**hA$_{2A}$ARs** **EC$_{50}$ (nM)**[c]	**hA$_{2B}$ARs** **EC$_{50}$ (nM)**[d]	**hA$_3$ARs** ***K*$_i$ (nM)**[e]
44	H	> 10000 (10%)	> 10000 (32%)	> 10000 (18%)	> 10000 (10%)	> 10000 (12%)
45	F	> 10000 (8%)	> 10000 (25%)	> 10000 (5%)	> 10000 (7%)	> 10000 (9%)
46	OCH_3	> 10000 (31%)	> 10000 (34%)	> 10000 (10%)	> 10000 (8%)	70 ± 6
47	$OCH_2CH_2OCH_3$	147 ± 11	682 ± 53	> 10000 (29%)	> 10000 (11%)	293 ± 27
48	OBn	243 ± 21	745 ± 62	>10000 (23%)	>10000 (13%)	37 ± 4
49	O(4-Cl)-Bn	8.12 ± 0.91	33 ± 4	52 ± 5	927 ± 86	36 ± 4
50	O(4-F)Bn	45 ± 4	235 ± 18	432 ± 37	> 10000 (9%)	43 ± 5
51	O(4-CF_3)-Bn	4.52 ± 0.42	24 ± 2	38 ± 3	866 ± 82	39 ± 4

52	OCH_2(4-Pyr)	> 10000 (29%)	> 10000 (6%)	> 10000 (8%)	> 10000 (7%)	248 ± 26
53	$O(CH_2)_3Ph$	3.63 ± 0.32	16.32 ±1.57	27 ± 3	389 ± 37	62 ± 7
54	$OCH_2COOCH_2CH_3$	75 ± 7	52 ± 5	74 ± 7	> 10000 (27%)	437 ± 42

[a]Displacement of specific [^{3}H]CCPA binding in membranes from hA_1CHO cells. [b]Displacement of specific [^{3}H]CGS21680 binding in membranes from hA_{2A}CHO cells. [c]Potency (EC_{50}) of examined compounds to stimulate cAMP levels in hA_{2A}CHO cells. [d]Potency (EC_{50}) of examined compounds to stimulate cAMP levels in hA_{2B} CHO cells. [e]Displacement of specific [^{125}I]AB-MECA binding in membranes from hA_3CHO cells. The values are expressed as the mean ± SEM, n=3-6 independent experiments. In parentheses are reported the % of inhibition to hA_1, A_{2A} , A_{2B} and A_3 CHO cells.

Table of Contents graphic